
GAZİ ÜNİVERSİTESİ
Gazi
1926

HARMONIC RESPONSIBILITY DETERMINATION AT A POINT OF COMMON COUPLING OF THE ELECTRICITY GRID USING WAVEFORM CORRELATION BASED ANALYSIS METHODS

A THESIS SUBMITTED TO
THE GRADUATE SCHOOL OF NATURAL AND APPLIED SCIENCES
OF
GAZİ UNIVERSITY

BY

Mustafa ÇALIŞKAN

IN PARTIAL FULFILLMENT OF THE REQUIREMENTS
FOR
THE DEGREE OF DOCTOR OF PHILOSOPHY
IN
ELECTRICAL ELECTRONIC ENGINEERING

AUGUST 2023

ETHICAL STATEMENT

I hereby declare that in this thesis study I prepared in accordance with thesis writing rules of Gazi University Graduate School of Natural and Applied Sciences;

- All data, information and documents presented in this thesis have been obtained within the scope of academic rules and ethical conduct,
- All information, documents, assessments and results have been presented in accordance with scientific ethical conduct and moral rules,
- All material used in this thesis that are not original to this work have been fully cited and referenced,
- No change has been made in the data used,
- The work presented in this thesis is original,

or else, I admit all loss of rights to be incurred against me.

Mustafa ÇALIŞKAN

09/08/2023

HARMONIC RESPONSIBILITY DETERMINATION AT A POINT OF COMMON COUPLING OF THE ELECTRICITY GRID USING WAVEFORM CORRELATION BASED ANALYSIS METHODS

(Ph. D. Thesis)

Mustafa ÇALIŞKAN

GAZİ UNIVERSITY

GRADUATE SCHOOL OF NATURAL AND APPLIED SCIENCES

August 2023

ABSTRACT

The goal of this thesis is to present a novel approach for distinguishing the distinct contributions of harmonic current and voltage from separate Electric Arc Furnace (EAF) systems supplied by a Point of Common Coupling (PCC). This approach identifies the unique harmonic current and voltage contributions of each EAF system by evaluating the waveforms of the PCC voltage and feeder current at each harmonic frequency. Due to the operational principles of EAFs, PCCs that supply power to several EAF plants typically encounter a high degree of current and voltage harmonic components, including uncommon ones. To treat these PCC harmonics efficiently, it is critical to differentiate the precise contributions from each EAF system fed by the PCC. The essential idea behind the approach is that the cumulative influence of voltage drops on the power supply system's source-side impedance induced by individual feeder currents results in the harmonic voltage across the PCC. The proposed technique computes the individual contribution of each EAF plant removing the requirement to monitor supplemental feeder currents to determine the EAF plant's contribution. The proposed technique's validity is assessed using synthetic data generated in a simulated environment. Furthermore, the method's performance is compared to that of other existing ways in the literature by using field measurements collected from a PCC that feeds electricity to several EAF units. Unlike earlier solutions to the similar problem the suggested technique does not require real-time impedance measurements or data from other feeders to calculate an individual feeder's contribution. The proposed method is refined to emphasize the impact of compensation systems installed in EAF plants and identify the issue of harmonic current sink in an affected plant with a strong compensation system by performing extra correlation calculations among the internal current measurements of the facility and the feeder currents. The suggested technique is easily implementable as a real-time solution for detecting harmonic contributions, leveraging power quality analyzers with synchronized feeder current and voltage data measurements.

Science Code	:	90524
Key Words	:	Power quality, power system harmonics, electric arc furnace
Page Number	:	81
Supervisor	:	Prof. Dr. Mehmet ÇİYDEM
Co-Supervisor	:	Prof. Dr. Özgül SALOR DURNA

DALGA FORMU İLİNTİSİNE DAYALI ÇÖZÜMLEME YÖNTEMLERİ KULLANARAK ELEKTRİK ŞEBEKESİNİN ORTAK BAĞLANTI NOKTASINDA HARMONİK SORUMLULUĞUN BELİRLENMESİ

(Doktora Tezi)

Mustafa ÇALIŞKAN

GAZİ ÜNİVERSİTESİ
FEN BİLİMLERİ ENSTİTÜSÜ

Ağustos 2023

ÖZET

Bu tez çalışmasının amacı, ortak bağlantı noktasından (OBN) beslenen elektrik ark ocağı sistemlerinin (EAO) bireysel harmonik akım ve gerilim katkılarını belirlemek için yeni bir yaklaşım sunmaktır. Yaklaşım, OBN geriliminin ve besleyici akımın her harmonik frekansında dalga şekli korelasyon hesaplarına dayanmaktadır. EAO'larının çalışma prensipleri nedeniyle, birden fazla EAO tesisi besleyen OBN'ları genellikle yüksek akım ve gerilim harmonik bileşenleri, özellikle karakteristik olmayanlardan etkilenmektedir. OBN'nda akım ve gerilim harmoniklerine karşı etkili önlemler almak için, farklı EAO'ları besleyen bir OBN'ndaki bireysel harmonik katkıları ayırt etmek gerekmektedir. Metodun temel fikri, harmonik gerilimin OBN üzerindeki toplam etkisi olarak, ayrık besleyici akımlar tarafından indüklenen şebeke sisteminin kaynak tarafı empedansı üzerindeki gerilim düşümünün kümülatif etkisinin bir sonucu olduğu gerçeğine dayanmaktadır. Önerilen yaklaşım, her bir EAO tesisinin harmonik katkısını ayrı ayrı hesaplamak için kullanılabilir. EAO tesisinin harmonik katkısını belirlemek için ek fider akımlarının ölçülmesi gerekmemektedir. Simülasyon ortamında üretilen sentetik veriler, önerilen yöntemi doğrulamak için kullanılmıştır. Yöntemin performansı daha sonra çok sayıda EAO birimine hizmet veren OBN'lerden alınan ölçümler kullanılarak literatürdeki diğer önerilen yaklaşımlarla karşılaştırılmıştır. Bu problem için daha önce yayınlanmış birkaç çözüm önerisinin aksine, önerilen yöntem, tek bir besleyicinin katkısını hesaplamak için gerçek zamanlı empedans ölçümleri ve diğer besleyicilerden alınan ölçümleri gerektirmemektedir. Önerilen yaklaşım, EAO tesislerinin kompanzasyon sistemlerinin etkilerini vurgulamak ve besleyici akımları ile tesis içi akım ölçümleri arasında ek korelasyon hesaplamaları kullanarak güçlü bir kompanzasyon sistemi ile etkilenen bir tesisin harmonik akım yutma problemini belirlemek için geliştirilmiştir. Önerilen yaklaşım, halihazırda senkronize gerilim ve besleyici akım dalga formu ölçümlerini içeren güç kalitesi analizörleri ile harmonik katkıları belirlemek için gerçek zamanlı bir araç olarak kolayca uyarlanabilir.

Bilim Kodu : 90524
Anahtar : Güç Kalitesi, güç sistemi harmonikleri, elektrik ark ocağı
Sayfa Adedi : 81
Danışman : Prof. Dr. Mehmet ÇİYDEM
İkinci Danışman : Prof. Dr. Özgül SALOR DURNA

ACKNOWLEDGEMENTS

I would like to thank Professor Mehmet ÇİYDEM for his direction, counsel, broad expertise, and critical input during my research effort. I am very grateful for his important contributions to my thesis study.

I am grateful to my co-supervisor, Professor Özgül SALOR-DURNA, for her encouragement, recommendations, and unfailing faith in me throughout my study. Her encouragement and continued support were key factors in the study's success. I am eternally thankful for her advice, encouragement, and substantial contributions during my doctoral studies.

I'd like to thank Professor Nursel AKÇAM and Associate Professor Murat GÖL for their help, criticism, and suggestions throughout my academic career. I would also like to express my genuine gratitude to Professor Umut ORGUNER, Professor Hasan Şakir BİLGE, and Associate Professor Emre ÖZKAN for their valuable recommendations and helpful feedback throughout the evaluation of my thesis. I am especially thankful to Erinç ALTINTAŞ, Özgür ÜNSAR, Mustafa Kemal ŞAHAN for their substantial assistance and companionship during my thesis research.

I am thankful to TÜBİTAK SAGE for their academic support throughout my thesis study.

I dedicate this thesis to my dear grandmother, who recently passed away. She was a constant source of love, support and inspiration in my life and it is with heavy heart that I dedicate this work to her memory. I also would like to dedicate my thesis to my beloved grandparents. I express my sincere sympathy to those who have been impacted by the recent earthquakes, including the individuals, families, and friends of those who lost their lives or were injured.

Last but not least, I wish to express my gratitude to my dear family for their unwavering encouragement and faith in me, particularly during this challenging period. I am fortunate to have such an incredible family and I love and appreciate each and every one of you.

TABLE OF CONTENTS

Page

Page

LIST OF TABLES

Table **Page**

LIST OF FIGURES

Figure **Page**

Figure **Page**

Figure **Page**

Figure **Page**

SYMBOLS AND ABBREVIATIONS

The symbols and abbreviations used in this study are presented below, along with their descriptions.

Symbols	Descriptions
s	Second
Hz	Hertz
MVA	Mega Volt Ampere

Abbreviations	Descriptions
APF	Active Power Filter
DFT	Discrete Fourier Transform
EAF	Electric Arc Furnace
FFT	Fast Fourier Transform
IEC	International Electrotechnical Commission
IEEE	Institute of Electrical and Electronics Engineers
KAMAG	Kamu Araştırmaları Destek Grubu
MATLAB	MATrix LABoratory
MVA	Mega Volt Ampere
PCC	Point of Common Coupling
PQ	Power quality
PSCAD	Power Systems Computer Aided Design
RMS	Root mean square
RMSE	Root mean square error
TEİAŞ	Türkiye Elektrik İletim A.Ş.
TS	Transformer Substation
TÜBİTAK	Türkiye Bilimsel ve Teknolojik Araştırma Kurumu

1. INTRODUCTION

Voltage harmonics at the point of common coupling (PCC) are a significant concern in power system research due to the presence of current harmonics generated by various power electronic systems and devices. Harmonic distortion poses a notable challenge in ensuring the stability and reliability of the power system. These harmonics are caused by nonlinear loads in the PCC, including arc welding equipment, electric arc furnaces (EAFs), electric motors, laddle furnaces and heavy industrial transformer stations. These loads produce electrical current at harmonic and interharmonic orders leading to harmonic distortion in the voltage at the PCC.

Harmonic distortion in voltage can cause issues for devices like computer hardware, regulation devices, and protection relays, leading to reduced efficiency, mis-operation, and device damage resulting in economic losses. Laws and legal penalties are put in place to make consumers accountable for the distorted harmonics they create to the electrical network, urging them to take preventative measures to avoid power outages or harm to equipment for other consumers connected to the PCC.

As a result, harmonic distortion induced by harmonic-producing loads should be decreased. International standards, such as IEEE IEC Standards 519 [1] and 61000-3-6 [2] describe allowable harmonic interference levels.

Each source connected to the electrical grid should take measures to prevent the emission of harmful harmonic pollutants. However, determining which source is responsible for a harmonic voltage disturbance at the PCC is difficult when existing power quality correction systems are insufficient or nonexistent. This is because simply measuring the harmonic currents in the feeders is not enough to identify the responsible source(s).

As a result, precisely identifying harmonic pollution sources is critical in power system analysis, especially when big polluting loads like as EAFs are connected to the PCC. Accurate identification is necessary to ensure that corrective measures are taken at the appropriate locations.

Furthermore, it is typical to find a "victim-plant" that has the most powerful harmonic compensation mechanism that successfully filters the harmonic currents from both itself and also different sources supplied from the PCC. While analyzing feeder currents, the victim-plant may appear to have the highest harmonic current, while in fact it is just filtering out harmonics from other sources. This issue of the victim-plant is a persistent challenge for PCCs that must be addressed.

The first step in resolving harmonic issues at the PCC is typically to separate and distinguish between the harmonic impacts resulting from both the supply and the load side in previous research.

The method described in [3] for calculating power direction was one of the first techniques for detecting the source of harmonics however it has been shown to have limitations and may provide inaccurate results in some cases as stated in [3].

Two alternative harmonic oriented methodologies to determine the key causes of harmonics are the primary harmonic source recognition methodology [4] and another approach that utilizes the IEEE standard 1459-2000 [5]. These methods establish whether side of the PCC, the supply or the load, has a stronger influence on harmonic distortion. However, they do not provide information about the specific amounts of harmonics produced by individual sources connected to the PCC.

The study in [6] describes a quality engineering based harmonic responsibility specification approach. To determine the impedance of both the utility and load sides, a Norton equivalent circuit model is created. The computed impedances are then utilized to calculate the economic losses incurred by both the customer and the supplier side at the PCC.

The research in [7] investigates the customer side's responsibility for voltage distortion at the PCC and introduces harmonic responsibility method based on the Maclaurin series. The source of the distortion may be determined using this approach, but not the particular contributions from each source.

The findings presented in [8] defines and presents the elements influencing harmonic current contribution detection at the PCC for both the load and supply sides. Thevenin and Norton network models are used to derive utility and load side impedances in order to calculate the individual harmonic distortion at the PCC. To establish who is accountable for harmonic voltage at the PCC, only harmonic impedances on both the supply and load sides must be calculated. Each load's specific harmonic current participation has not been provided.

The research conducted in [9] proposes a method for establishing the accountability of harmonic producers for every bus and branch of an electrical grid utilizing current tracing approach. The results of applying this approach to the IEEE 9-bus topology reveal the harmonic current responsibility. [10] offers a technique for calculating the overall harmonic participation of each user and utilities using a combination of change-point monitoring, canonical correlation analysis and dynamically altered form context. The harmonic current participation for the supply and load sides is shown in the data presented within the IEEE 14 bus architecture. The harmonic current participation for each harmonic order is not shown in [9] or [10].

Other strategies for determining harmonic participations using power grid impedance models have been presented in the literature. In [11] and [12], for example, the impedance of the source and utility sides as seen from the PCC is computed in each 10-cycle data frame to determine the harmonic contributions of the load and utility. Harmonic current contributions of iron and steel (I&S) plants are calculated using IEC61000-4-7 and solving the circuit analysis of each feeder for the corresponding harmonic frequency [13]. Time synched current and voltage data measurement at the PCC and inside the loads are required for this approach. While these approaches produce correct findings, the immediate impedance calculation might cause time delays and heavy processing demands, making real-time power quality detection algorithms difficult to implement. Furthermore, to eliminate the requirement for expensive resistive-capacitive voltage transformer (RCVT), that offer accurate measurement of voltage at higher order harmonics [11], the solution in [12] needs measurements of current inside the facility. However, obtaining in-plant measurements often requires special permissions and procedures, which can be difficult to obtain.

The harmonic current vector approach in [14], the superposition and projection method in [15], and the RLC method in [16] are all impedance-based solutions aimed at identifying the harmonic source and responsibility at the PCC by calculating supply and load side impedance. These approaches can offer information on the harmonic contributions from both the utility and loads, but not on the specific contributions from each load.
Recent studies have focused on solutions that utilize waveform correlation. One such example is found in [17], where harmonic source identification is based on the correlation between voltage and current waveforms, allowing for the determination of harmonic responsibilities for specific frequencies. However, this method does not enable the calculation of the amount of harmonic contribution levels. The amount of contribution from nonlinear loads towards harmonic distortion is not determined in this research.

Another study, described in [18], uses current and voltage data correlation coefficient for utility and loads in order to assess if the circuit has any harmonic sources. The circuit model is demonstrated and the system's harmonic impedance is calculated using linear regression approach. To determine the harmonic accountability of loads, supply and load side impedance must be computed. However, the method's processing complexity renders it unsuitable for real-time applications.

Waveform correlation method is used in [19] to reveal errors in generating harmonic responsibility. Harmonic current contribution of the upstream and demand side is calculated using the amplitudes and phasor angles of the measured data, as well as the correlation value of the time domain current and voltage data. A false decision detection approach is also presented to discover the true origins of both the supply and load side harmonics. This approach, unlike others, does not involve the computation of utility and load side impedance, making it more appropriate for real-time applications. The study's goal is to identify the loads that are causing the harmonics, not how much every single load participates to the overall harmonics within the PCC.

Although numerous approaches have been offered in the literature, briefly mentioned above, there is no method that works under all conditions and finds out which load generates how many harmonics. This thesis contains methods developed to fill the gap in this field.

2. PROBLEM DEFINITION

An EAF is a furnace that heats a material using an electric arc. The size of EAFs can range from small ones with a capacity of a few grams used in laboratory and dental applications to large ones with capacities of up to 400 tons used in steelmaking. EAFs can produce extreme temperatures, with industrial units reaching up to 1,800°C and laboratory units reaching 3,000°C or higher. The scrap material is immediately exposed to the electric arc, and current passes through it from the furnace terminals. EAFs vary from induction furnaces in that the charge is heated by eddy currents rather than induction [20]. Figure 2.1 shows a 135-tonne capacity and 180 MVA AC EAF.

Figure 2.1. A 135 tons capacity and 180-MVA EAF [21].

The EAF has specific properties that make it different from other types of furnaces. These properties are caused by the rapidly changing active and reactive power demands, the existence of multiple harmonics and interharmonics, and fundamental frequency fluctuations.

Figure 2.2 shows a diagram that includes a PCC with an induction furnace, arc furnace, industrial loads and urban loads all shown in a single-line illustration.

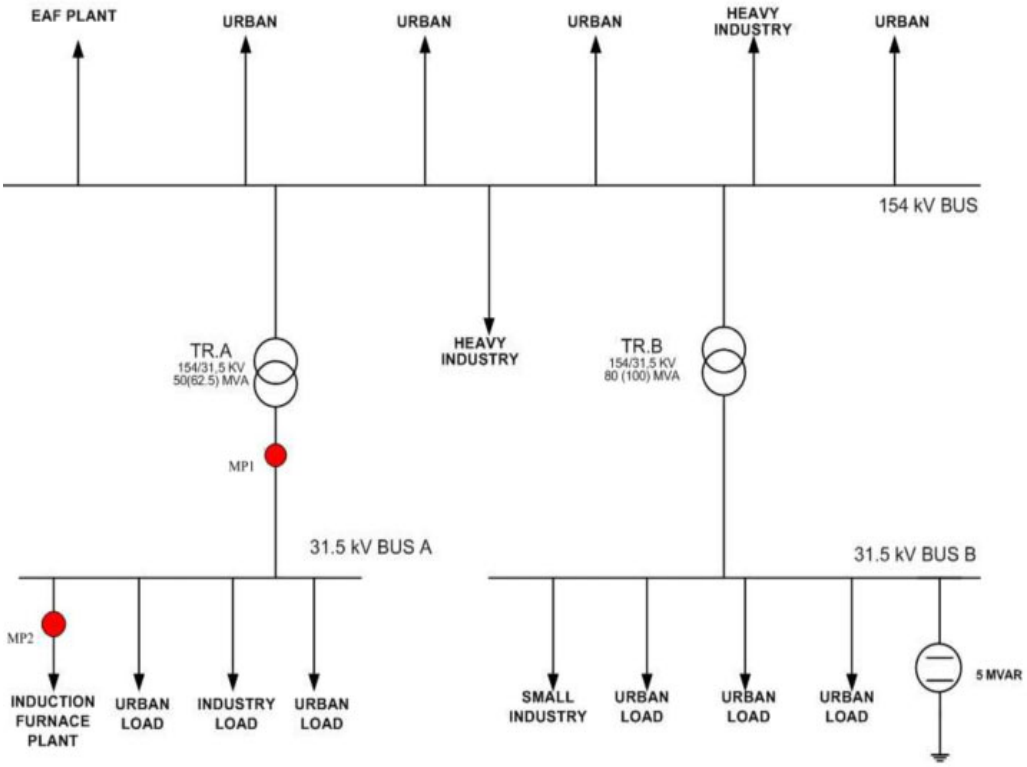

Figure 2.2. Single line illustration of a PCC with induction furnace, arc furnace, industry loads and urban loads [22].

The use of EAFs in the power system can result in several negative consequences, including possible damage to power system units, harmful impacts on neighboring industrial and urban plants connected to the PCC, over voltages and over currents due to parallel or series resonances, and reduced productivity due to voltage drop at the PCC caused by reactive power consumption by the EAFs. Furthermore, because of nonlinear and stochastic behavior of EAFs, the harmonic sinking problem, in which a victim plant with an efficient compensating mechanism absorbs all harmonics from other power plants linked to the PCC, might arise. To solve these difficulties, the research in this thesis work uses waveform correlation analysis techniques to measure the harmonic current and voltage outputs of EAFs supplied from the PCC.

2.1. Outline of the Thesis

In this thesis study, a novel approach is developed using the correlation between the PCC voltage and the currents of the feeders to detect the source of harmonics in the EAF plants that receive power from the PCC.

The technique proposed leverages the connection established between the correlation coefficient of the PCC voltage and the current data of the feeders and the extent to which each EAF plant fed by the PCC contributes to the harmonic voltage and current.

The core concept stems from the understanding that the harmonic voltage present at the PCC is a sum of the voltage drops across the power system's source side impedance induced by each separate feeder current.

This technique has the benefit of not requiring the calculation of the client-side impedance, and its computing requirements are substantially lower as compared with the other methods available in the existing literature. A further benefit of this technique is that just the related feeder current of a single plant is required to establish its contribution, as opposed to the experiments reported in [11] and [12], which required all of the PCC's feeders.

The suggested technique was validated by executing circuit simulations incorporating harmonic producing loads and the PCC supply side in both PSCAD and MATLAB. The suggested approach is used to real-time field data from different substations supporting a variety of EAF devices, yielding encouraging results for identifying harmonic voltage and current contributions in PCC.

The proposed method was further developed to take into account the impact of the compensator devices in EAF plants. This enhanced technique can identify the issue of a victimized facility having an excessively strong compensator mechanism and sinking harmonic current by performing extra correlation calculations between feeder currents and inside facility measurements of current.

The following are the contributions and major characteristics of the suggested approach.

- To avoid the real-time computation of load and utility side impedances from real time measurements of voltage and current signals, a harmonic contribution detection approach that utilizes waveform correlation evaluation is presented.

- Based on real-time current and voltage measurement data, the proposed technique successfully detects the separate contribution of harmonic voltage and current from each I&S facility provided by the PCC for each harmonic frequency.

- The proposed technique additionally employs waveform signal correlation to calculate the contribution of the load and supply side harmonics to the I&S plant's shunt harmonic filter. In addition, it can detect the problem of harmonic current sink.

- Utilizing inside facility or PCC voltage and current data, the proposed approach accurately finds the substations responsible for harmonics. This information can be used to identify companies that exceed legal limits and take necessary measures to mitigate the issue.

- Additionally, the results of this thesis work have been published in various journal and conference publications listed in references between [23-27], respectively.

The thesis is organized as follows:

The first and second sections of Chapter 3 demonstrate how to calculate harmonic current responsibility using waveform correlation analysis. The third section demonstrates validation of the suggested technique in simulation environment with PSCAD and MATLAB. The fourth section uses synchronous real time measured field data from several substations to demonstrate the efficacy of the suggested approach.

The mathematical relationship between the correlation of voltage and current waveforms and the size of the voltage harmonic contribution at a PCC is established in Chapter 4.

Chapter 5 is broken into two sections. In the first section, the waveform correlation-based voltage harmonic contribution detection method which was derived in Chapter 4 is tested and verified through simulation using PSCAD and MATLAB. The second part showcases the implementation of this method on real-life field measurements taken at a PCC feeding EAFs, with results being illustrated and analyzed.

In Chapter 6, the supply and load side contributions to a plant's shunt harmonic filter are represented using different scenarios and evaluated using the waveform correlation approach given in Chapter 4. This is done to investigate the case of victim I&S facilities equipped with powerful harmonic compensators.

The results and fundamental assertions of the study are summarized in the last chapter of the research work, and the future path of research in the same subject is considered.

3. HARMONIC CURRENT RESPONSIBILITY DETERMINATION WITH WAVEFORM CORRELATION

3.1. Brief Overview of the Proposed Method

This chapter introduces a unique approach for identifying harmonic responsibility that makes use of the correlation between feeder currents and PCC voltages measured at the same time. Harmonic spectrum is estimated using ten-cycle frames of both PCC voltage and load current signals collected concurrently at transformer substations serving EAF facilities, in compliance with the IEC 61000-4-7 standard [13]. PQ+ power quality analyzers developed by Turkey's Power Quality Project [28] are used to capture real-time field data.

Following that, the waveform correlation technique described in [19] is applied to calculate the harmonic participations of EAF plants connected to the PCC, with the method being run independently for each frequency component. Although this study focuses on harmonic components with comparatively notable amplitudes, the suggested approach is applicable to any frequency component including interharmonic analysis.

Utilizing the identical collection of data, the harmonic current participation results are compared with the outcomes from impedance calculation-based methods reported in [11] and [12]. The study demonstrates that the suggested technique may obtain comparable findings without requiring instantaneous measurements of source and load impedance giving it an advantage over other methods. Figure 3.1 depicts the signal processing mechanism utilized by the proposed harmonic current accountability identification technique.

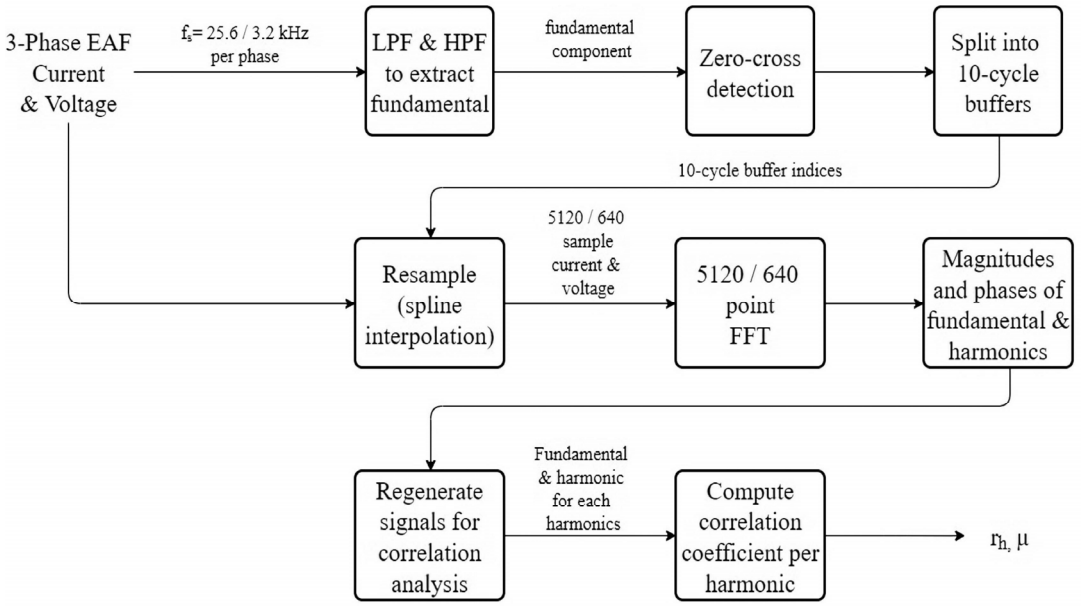

Figure 3.1. The block diagram of the proposed method for signal processing.

The suggested approach works as following way:

1. PQ+ analyzers developed as part of Turkey's Power Quality Project collect current and voltage measurements simultaneously from a transformer facility supplying arc furnace units. The sampling rate of the data is either 25.6 kHz or 3.2 kHz, depending on the PQ monitoring device's sampling frequency. Nonoverlapping windows of ten cycles, which correspond to equate to about 200 ms data segments for 50 Hz fundamental frequency power system, are utilized as data inputs for Discrete Fourier Transform (DFT) calculation in accordance with the recommendation of IEC Standard 61000-4-7 [13].

2. To accurately determine the frequencies of the recorded voltage and current data through zero-crossing, it is important to remove frequency components that deviate from a pure sinusoidal shape. To achieve this, the instantaneous current and voltage signals from the load feeders undergo filtering with a band-stop filter in MATLAB, with cut-off frequencies set to 45 Hz and 65 Hz. The filter is applied to eliminate frequency parameters that differ from the grid fundamental frequency of 50 Hz, which may cause distortion in the analysis.

3. A good assessment of the fundamental frequency is required to eliminate these spectral estimation mistakes. The precise fundamental frequency is calculated by correcting the initial and final zero-crossings, as shown in [29]-[30]. This adjustment is shown in Figure 3.2 on a zero-crossing scenario. The precise zero-crossing can be identified by performing a linear interpolation across the two data points, as shown in Figure 3.2, in which X represents each sample of the signal and O represents the signal's true zero-crossing, which is calculated both at the start and end of the 10-cycle time frame for accurate fundamental frequency assessment [29].

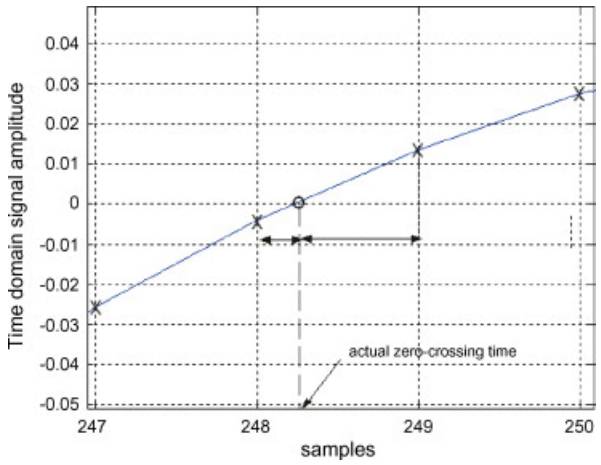

Figure 3.2. Zero-crossing correction [29].

4. For each ten-cycle length, the zero crossings of the voltage and current data are utilized to calculate the precise fundamental frequency [29]-[30]. The results obtained are then reproduced utilizing cubic spline interpolation for fitting into either 5120 points (512 point every period at 25.6 kHz sampling rate) or 640 points (64 points every period at 3.2 kHz sampling rate) sampling frames across the ten cycles of the fundamental interval. This enables for calculations using DFT with no spectrum leaking, and the resulting frequency precision is equivalent to fs/10, wherein fs is the system's momentary fundamental frequency. The tenth DFT point correlates to the nominal frequency, fs, while the twentieth DFT point refers to the second harmonic order, and thereafter [13]. By changing the ten-period duration to the identical amount of DFT points, the spectrum leaking impact of the DFT process is reduced [29].

5. In this study, the subgroup computing technique provided in the IEC-61000-4-7 standard [13] is utilized to compute the harmonic and interharmonic elements of both voltage and current signals. Because the values of the frequency elements beyond the thirteenth harmonic are often small in actual power platforms, the amplitudes and phase of the nominal frequency and greater-order harmonics are calculated up until the thirteenth harmonic order. If necessary, the same method can be done to all harmonic orders.

6. For both current and voltage data, the amplitudes and phase of the harmonics are calculated. Only the nominal frequency and the studied harmonic frequency portion of time domain current as well as voltage signals are rebuilt. For every synchronized ten period current and voltage sinusoidal frame couple, the coefficient of Pearson's correlation [31] is computed. In the end, the greatest correlation value derived from the generated sinusoidal correlation coefficients is chosen as the final result.

7. Utilizing the correlation coefficient and amplitudes of the basic frequency and particular harmonic frequencies specified in [19], the approach determines the harmonic injections of demands and the resulting distortion ratio for incorrect assessment identification. The results show that the technique can function in real-time on PQ+ analyzer and estimate the harmonic current accountability of loads well.

The IEC-61000-4-7 calculation techniques for harmonics and interharmonics are summarized in the following section.

3.1.1. IEC-61000-4-7 Harmonic and interharmonic computation methods

Harmonic and interharmonic groups, subgroups, and single-line harmonic frequency computation are three methodologies for quantifying waveform distortions described in the IEC-61000-4-7 standard [13]. The parts that follow merely outline these three strategies.

Harmonic and interharmonic groups computation

The harmonic group's rms value is computed utilizing harmonics and their neighboring interharmonics. The square root of the sum of the squared values of a harmonic and its neighboring interharmonics according to the time frame, i.e., for 50 Hz networks with a resolution of 5 Hz as stated in Equation 3.1. Ck represents the rms amplitude of the kth spectral element derived from DFT.

$$G_{g,k} = \sqrt{\frac{C_{k-5}^2}{2} + \sum_{i=-4}^{4} C_{k+i}^2 + \frac{C_{k+5}^2}{2}} \tag{3.1}$$

Interharmonic group for the 50 Hz power network is defined as in Equation 3.2.

$$G_{ig,k} = \sqrt{\sum_{i=1}^{9} C_{k+i}^2} \tag{3.2}$$

C_{k+i} is the $(k+i)^{th}$ DFT amplitude, and these are the interharmonic elements between the $(n)^{th}$ and $(n+1)^{th}$ harmonics (e.g., nine consecutive FFT points between 105 Hz and 145 Hz for second and third harmonic values).

Computation of harmonic and interharmonic subgroups

Harmonic subgroup is computed utilizing the harmonic component and its preceding and subsequent DFT components. The calculated RMS value is the square root of the sum of the values that have been squared of the harmonic components as given in Equation 3.3. The consequences of harmonic amplitude and phase variations are partially mitigated by the subgroup calculation method.

$$G_{sg,k} = \sqrt{\sum_{i=-1}^{1} C_{k+i}^2} \tag{3.3}$$

The interharmonic subgroup is calculated using the interharmonic components between two integer harmonic frequencies, excluding those immediately adjacent to those harmonic frequencies, as in Equation 3.4.

$$G_{isg,k} = \sqrt{\sum_{i=1}^{9} C_{k+i}^2} \tag{3.4}$$

Single-line harmonic frequency computation

When calculating the harmonic frequency of a single line, the FFT with a resolution of 5 Hz is applied directly to the measured ten-cycle waveform of line voltage and current waveforms in accordance with IEC 61000-4-7. Using this method, both the phase and amplitude values for the fundamental as well as harmonic frequencies are computed. Interharmonic components are not calculated. The harmonic spectrum of a single line and the representation of the harmonic and interharmonic subgroup and group computation is shown in Figure 3.3 provided in [32].

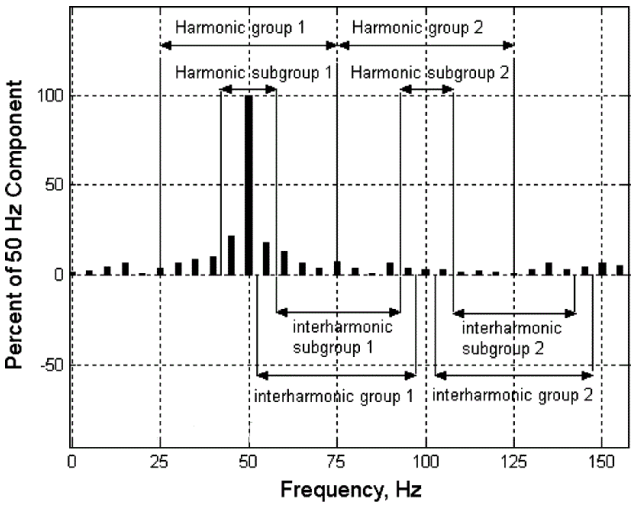

Figure 3.3. Presentation of the harmonic and interharmonic subgroup and group computations [32] specified in the standard IEC 61000-4-7.

The study uses the standard-recommended harmonic and interharmonic subgroup computation method to calculate harmonic spectra parameters for non-overlapping ten period evaluation frames. Time synched voltage and current data are filtered, and the zero crossings of the data are properly calculated.

Using these zero crossings, the nominal frequency is computed for each ten-period data frame. Non-overlapping ten cycle FFT frames are applied, and the amplitude and phase spectra of the nominal and higher frequency harmonics are calculated for utilization in waveform correlation evaluation, which is used to assess harmonic accountability. The next section describes the waveform correlation evaluation procedures involved in the proposed technique for finding harmonic contributions.

3.2. Identification of Harmonic Contributions with Waveform Correlation

This section covers how to identify a harmonic source of current on both the demand and utility ends. The approach for determining harmonic contributions in the present research relies on an analysis of correlation between observed voltage at PCC and feeder current. As a result, the following subsection addresses correlation computation briefly.

3.2.1. Correlation coefficient

Correlation coefficient is a measure of statistical significance that indicates the level of relationship between the dependent movements of two variables. The correlation coefficient has a range of -1 to +1, wherein -1 represents an ideal negative correlation, +1 represents an ideal positive correlation, and 0 represents no association between the movements of the two parameters.

$$r_{xy} = \frac{\sum_{i=1}^{n}(x_i - \bar{x})(y_i - \bar{y})}{\sqrt{\sum_{i=1}^{n}(x_i - \bar{x})^2}\sqrt{\sum_{i=1}^{n}(y_i - \bar{y})^2}} \tag{3.5}$$

Equation 3.5 is employed to calculate the Pearson correlation coefficient [31] among the two sets of information, whereby x_i, y_i (i = 1, 2..., N) represent the information instances, the total number of array elements is N and $\bar{x}$ and $\bar{y}$ represent the dataset averages. When the correlation value between the current and voltage of a linear load is calculated, it is generally close to one, suggesting a strong positive relationship, but the value of correlation for nonlinear loads is lower.

A significant correlation value for a load considered to be causing harmonics may signal wrongly that the load in question does not contribute to harmonics in the electrical grid.

3.2.2. Waveform correlation for harmonic liability identification

Equations 3.6 and 3.7 define both voltage data recorded at PCC and the current data recorded at particular feeder. The equation includes time-varying current and voltage amplitudes such as U_1, U_h,I_1,I_h and phase components such as θ_{u1},θ_{uh},θ_{i1}, θ_{ih}

$$u(t) = \sqrt{2}U_1 \sin(\omega t + \theta_{u1}) + \sum_{h=2}^{\infty} \sqrt{2}U_h \sin(h\omega t + \theta_{uh}) \tag{3.6}$$

$$i(t) = \sqrt{2}I_1 \sin\left(\omega t + \theta_{i1}\right) + \sum_{h=2}^{\infty} \sqrt{2}I_h \sin\left(h\omega t + \theta_{ih}\right) \tag{3.7}$$

The sampled current and voltage data may be represented as given in Equation 3.8, wherein k represents sample indexes while N indicates total length of examined data. $u_h[k]$ and $i_h[k]$ denote data sequences for voltage and current, respectively.

$$\left\{\begin{array}{l} u_h[k] = \sqrt{2}U_1 \sin\left(\dfrac{2\pi}{N}(k-1) + \theta_1\right) + \sqrt{2}U_h \sin\left(\dfrac{2\pi h}{N}(k-1) + \theta_{uh}\right) \\ i_h[k] = \sqrt{2}I_1 \sin\left(\dfrac{2\pi}{N}(k-1) + \theta_1\right) + \sqrt{2}I_h \sin\left(\dfrac{2\pi h}{N}(k-1) + \theta_{ih}\right) \end{array}\right\} \tag{3.8}$$

The identity in Equation 3.9 can be used to simplify the computation of the relationship between the voltage and current readings. The sum of the sinusoidal components for a harmonic signal that is uniformly recorded in its associated integral period is zero [19]. Therefore, the equation can be expressed as,

$$\sum_{k=0}^{N-1} A \sin\left(\frac{2\pi hk}{N} + \varphi\right) = 0, (k = 0,1 \cdots N-1) \tag{3.9}$$

wherein A is the waveform's amplitude, h represents harmonic index, k shows sampling point, N denotes signal duration and primary phase is φ.

In Figure 3.1, the resampling block guarantees that both the voltage and current signals are sampled evenly during the ten-cycle data frame. For an inductive load, Equation 3.5 yields Equation 3.10 for the correlation value across the current and voltage data for the h^{th} harmonic order by putting Equation 3.8 into Equation 3.5 and applying Equation 3.9 [19].

$$r_h = \frac{1 + (U_h / U_1) \times (I_h / I_1) \times \cos\left(\theta_{uh} - \theta_{ih}\right)}{\sqrt{[1 + (U_h / U_1)^2] \times [1 + (I_h / I_1)^2]}} \tag{3.10}$$

Equations 3.9 and 3.10 may be used to compute both harmonic current participation of the demand and the resulting distortion ratio at a given harmonic order, as shown in Equation 3.11 [19].

$$\begin{cases} I_{he} = I_1 \times \sqrt{\dfrac{1}{r_h^2 (1 + (U_h / U_1)^2)} - 1} \\ \mu_h = \dfrac{I_{he}}{I_h} \end{cases} \tag{3.11}$$

Here, $\mathrm{I_1}$ represents the demand's nominal frequency current magnitude, $\mathrm{U_1}$ and $\mathrm{U_h}$ are the nominal frequency and h^{th} harmonic order voltage magnitudes at PCC, $\mathrm{r_h}$ represents the correlation value of the collected current as well as voltage data at the h^{th} harmonic order, $\mathrm{I_{he}}$ is the computed harmonic participation of the demand for the h^{th} harmonic order, and μ_h is the misjudgment identification proportion of the calculated value (I_{he}) to the original magnitude (I_h) [19].

The subsequent procedures can be used to identify the current harmonic generated by loads using waveform correlation evaluation. Figure 3.4 depicts the algorithm for finding the participation of the h^{th} order harmonic current (I_{he}).

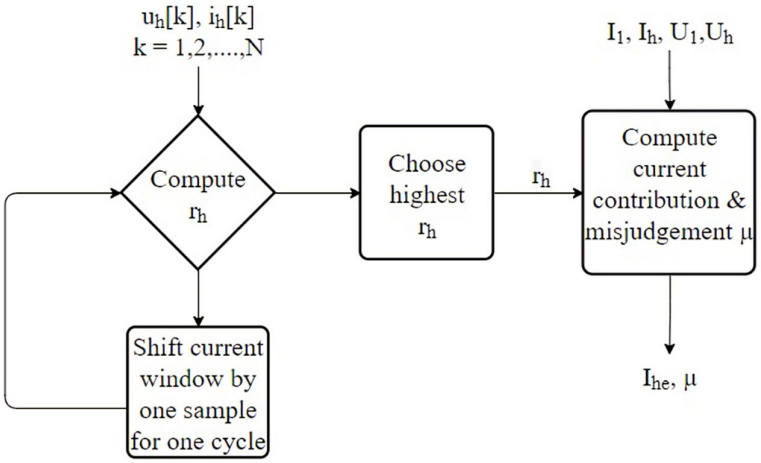

Figure 3.4. Contribution of harmonic current to the h^{th} harmonic I_{he} calculation.

The process for identifying harmonic current accountability and detecting errors in judgment using this approach is described in the following steps, as depicted in Figure 3.4.

- The amplitude and phase spectra of the current and voltage of the targeted loads are obtained for every ten-period distinct DFT frame utilizing IEC-61000-4-7 subgroup computing technique. This method produces values for I_1, I_h, U_1, and U_h, which correspond to the nominal and h^{th} harmonic frequencies, respectively. A resampling approach is used to prevent spectral leaking caused by frequency variation. Details of this method are provided in Figure 3.1.

- Using the harmonic spectral results obtained in the previous stage, generate time domain voltage and current signals incorporating the calculated fundamental and higher frequency harmonics using the equation provided in 3.8.

  The Pearson correlation value (r_h) between the reconstructed voltage and current data is calculated using the formula described in Equation 3.5. The numerical values of the correlation coefficients are computed over sliding frames, with the ten period voltage data window fixed and the current data window moving one sample at a time. This shifting procedure is performed for one nominal frequency period. The final result for each ten-cycle frame with the greatest correlation value is chosen.

- The amplitude and phase spectra results acquired in the initial phase, as well as the correlation value derived in the preceding step using Equation 3.11, are used to calculate the participation of the harmonic loads and the resulting distortion ratio results for the investigated harmonic orders.

3.3. Approval of the Suggested Technique

This part describes how the suggested strategy is validated using the PSCAD and MATLAB simulation tools. As shown in Figure 3.5, the validation procedure comprises simulating three harmonic-generating loads along with a utility side current source with harmonic injections. The impedance values depicted in Figure 3.5 closely resemble the simulation values shown in the circuit diagram mentioned in [11]. This comparison aims to validate the algorithm's outcomes against the impedance calculation-centric approach within a simulated setting.

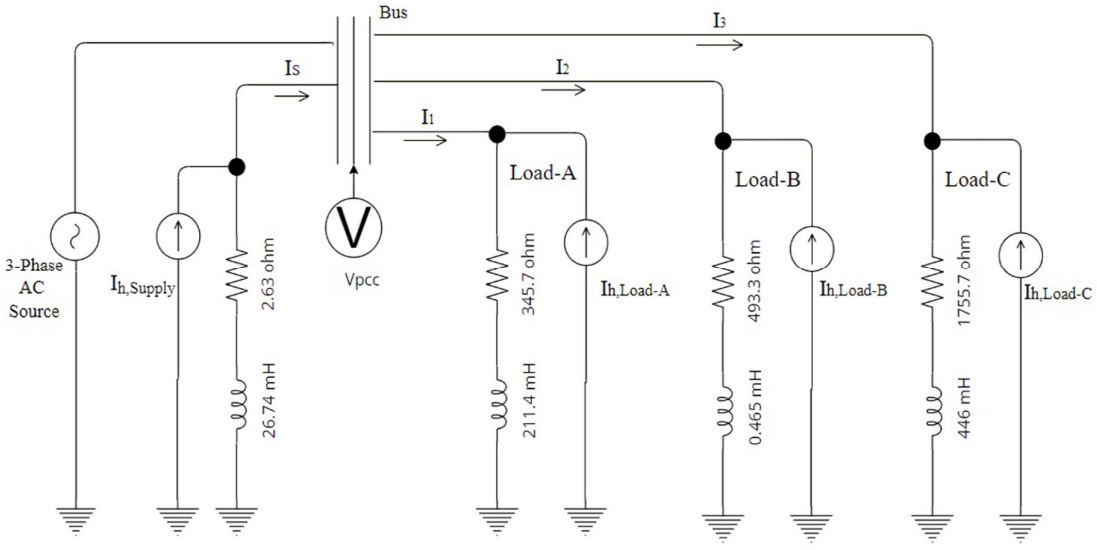

Figure 3.5. A PSCAD circuit schematic is created to test the recommended approach.

The subsequent procedures are used to validate the suggested technique:

1. Table 3.1 shows the magnitudes of the present harmonic emitters. $I_{h,Supply}$, $I_{h,Load-A}$, $I_{h,Load-B}$, and $I_{h,Load-C}$ are used as input for the computer simulation in the PSCAD program to assess the recommended strategy. Table 3.1 shows the harmonic frequency levels studied: n = 2, 3, 5, and 7. Without sacrificing generality, the phase values of all inputs and harmonic levels are set to zero. At the PCC, the default utility voltage V_{pcc} has been set to 154 kV, and the nominal frequency of the whole system is set to 50 Hz. Circuit simulation output is produced at a frequency of sampling of 25.6 kHz for one minute. Based on the current values provided in Table 3.1, the supply side and Load-A produce harmonics at a frequency of 100Hz. At 150 Hz, only Load-B generates harmonics, while at 250 Hz, only Load-C contributes to current harmonics. Lastly, at 350 Hz, both Load-A and Load-B introduce current harmonics into the system. The primary objective is to differentiate the source of harmonics in different scenarios, simulating real-time situations.

Table 3.1. PSCAD simulation input parameters f: Harmonic Frequency (Hz), I: Current Harmonics RMS Amplitude (Ampere)

Frequency (Hz)	$I_{h,Supply}$ (A)	$I_{h,\ Load-A}$ (A)	$I_{h,Load-B}$ (A)	$I_{h,Load-C}$ (A)
100	100	100	-	-
150	-	-	200	-
250	-	-	-	300
350	-	40	20	-

2. The magnitude and phase spectra of the voltage and harmonic current sources are computed for each separate ten-period DFT frame utilizing the subgroup computation approach of IEC-61000-4-7. Table 3.2 summarizes the findings. Based on the data presented in Table 3.2, it's noticeable that the DFT amplitudes are more significant at frequencies where harmonic currents are generated compared to frequencies without harmonic loads. However, relying solely on DFT amplitudes is insufficient as they don't provide information about the number of harmonics introduced into the system.

Table 3.2. The recorded voltage and current signals' DFT amplitude spectra. f: Harmonic Frequency (Hz), V: PCC Voltage DFT Amplitude for each harmonic order (Volt), I: PCC Current DFT Amplitude for each harmonic order (Ampere)

Frequency (Hz)	V_{pcc} (V)	$I_{h,Supply}$ (A)	$I_{h,\ Load\text{-}A}$ (A)	$I_{h,Load\text{-}B}$ (A)	$I_{h,Load\text{-}C}$ (A)
50	$154.5*10^3$	$19.5*10^3$	440.30	315.50	85.20
100	117.30	123.20	110.50	0.33	0.04
150	135.80	25.50	0.74	222.12	0.07
250	472.70	25.55	0.88	0.78	335.50
350	43.250	4.45	42.75	20.75	0.045

3. Calculated DFT spectra of current and voltage are used by the suggested method's phases, which are given in Equations (3.8) - (3.11). The distortion ratio results of the suggested approach for each harmonic frequency are shown in Table 3.3. The distortion ratio is determined to be 0 at frequencies with no harmonic contribution, correctly identifying the harmonic responsibility of the load side and utility side for the relevant harmonic frequency.

Table 3.3. Findings on distortion ratios with regard to the harmonic frequency. f: frequency (Hz), μ_h : distortion ratio.

Frequency (Hz)	$\mu_{h,supply}$	$\mu_{h,Load\text{-}A}$	$\mu_{h,Load\text{-}B}$	$\mu_{h,Load\text{-}C}$
100	0.733	0.996	-	-
150	-	-	0.998	-
250	-	-	-	0.987
350	-	-	0.994	-

4. In a simulation environment, the suggested approach's reliability is compared to an approach described in [11] with regard to the RMSE for the harmonic contributions. The results for the frequency orders are shown in Tables 3.4 and 3.5. Since [11] computes the impedance for each frequency and achieves the findings via circuit modeling, the suggested method's RMSE is somewhat greater for some frequencies. The RMSE values of the two techniques, however, are extremely similar, and it is determined that the suggested method works well.

Table 3.4. The RMSE for the simulation findings acquired in the PSCAD experiment using the approach given in [11] for each harmonic order.

Frequency (Hz)	$RMSE_{supply}$	$RMSE_{Load-A}$	$RMSE_{Load-B}$	$RMSE_{Load-C}$
100	0.009	0.008	-	-
150	-	-	0.09	-
250	-	-	-	0.002
350	-	0.03	0.009	-

Table 3.5. The RMSE for the simulation findings acquired in the PSCAD experiment using the suggested technique for each harmonic order.

Frequency (Hz)	$RMSE_{supply}$	$RMSE_{Load-A}$	$RMSE_{Load-B}$	$RMSE_{Load-C}$
100	0.012	0.012	-	-
150	-	-	0.104	-
250	-	-	-	0.006
350	-	0.068	0.012	-

5. Because they compute the DFT spectra of time-synched voltage and current data, the suggested approach and technique provided in [11] are both simply implementable in software. Their computational complexity is equivalent, and both may be employed in PQ+ monitors to evaluate harmonic accountability for grid networks. The suggested approach is advantageous because it does not require impedance measurements, making it a faster method. Even though the proposed method may have a slight accuracy issue, it can be compensated for.

6. A pilot investigation is conducted to test the suggested approach for real-time field measurements using the simulated circuit displayed in Figure 3.5, which relied on a simplified design of the ISKENDERUN-2 converter substation depicted in Figure 3.6. This technique allowed the suggested solution to be tested in a simulated environment.

In the next section, the proposed method is going to be utilized with real time field measurements gathered from numerous electrical substations.

3.4. The Proposed Method's Implementation to Real Time Field Data

3.4.1. Results from ISK-2 Transformer Station

The ISK-2 converter station, located within Turkey's power transmission network, serves as the focal point for applying the proposed method to evaluate the associated data. As illustrated in Figure 3.6, this power station supplies energy to a variety of industrial facilities, including the AC arc furnace (Load-A), the iron and steel rolling mill factory and smaller manufacturing facilities (Load-B), and the DC arc furnace (Load-C). The other power sources, involving upper stream demands and utilities, are regarded to be on the supply side. The electrical simulation shown in Figure 3.5 is a minimized representation of the real transformer substation shown in Figure 3.6.

PQ+ analyzers [33] record on-line voltage and current data from each feeder at a sampling rate of 25.6 kHz per line to the MP_1, MP_2 and MP_3 measurement zones in Figure 3.6. The cumulative influence of the feeders energizing the busbar is illustrated in Figure 3.6 as the voltage source Es with a series impedance of the source $Zs = Rs + jXs$, according to Thevenin circuit theorem.

For this study, one minute of Phase-A data was collected and used to identify the harmonic sources. The transformer is activated during the time span between the twenty-second and thirty-first seconds within a given minute. When this 154/31.5 kV transformer is turned on, the system has a brief period of instability, notably during the first operation of the arc furnaces attached to the PCC. During this time, it is difficult to determine the phase separation between the current and voltage nominal components using the zero-crossing approach of waveforms. This problem persists for several periods after the transformer is turned on.

According to the research published in reference [35], a threshold value of 15% for the percentage of the second harmonic value to the nominal harmonic value was determined to detect whether the converter is powered. Utilizing this approach, it was found that the transformer in The DC EAF plant (Load-C) was triggered for the first time between the twenty-second and the thirty-first seconds of the data recording period, while the other power converters were already operational.

Consequently, this temporal period for simulation findings was subtracted from field data collected from Load-A, Load-B, and Load-C.

This research's data is identical to that utilized in a prior work released in [11]. The identical a minute investigation period was utilized to contrast the findings of this study to those of [11].

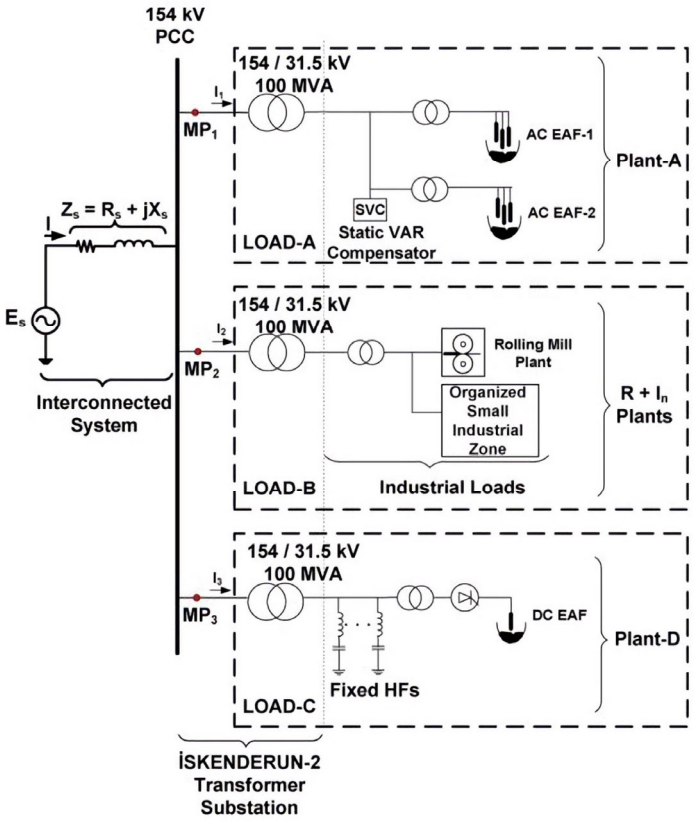

Figure 3.6. Simplified Model of ISKENDERUN-2 transformer substation [22].

The harmonic current accountability of Load-A, Load-B, and Load-C on the 2nd, 3rd, 5th, and 7th harmonics is calculated using correlation analysis and Equation 3.11. The resulting data are shown in Figures 3.7, 3.9 and 3.11, respectively. The analysis only covers these specific harmonic orders as they have the highest amplitudes for EAF systems. Nevertheless, the proposed method is applicable to other harmonics and interharmonics.

The figures presented yield the following summary of results:

1. According to the data in Figure 3.7 (a), Load-A is responsible for the bulk of the identified second harmonics in current at MP_1. Similar results were obtained for the second harmonic currents of Load-B and Load-C, as illustrated in Figures 3.9 (a) and 3.11 (a). The data reveal that the remaining loads injected a negligible amount of second current harmonics into the corresponding feeds.

2. The impacts of Load-A, Load-B, as well as the utility end, are bigger than the measured third current harmonics at MP_1 and MP_2, as illustrated in Figures 3.7 (b) and 3.9 (b). The overall measured third-harmonic current magnitude drops because the phase angle between the contributions from Load-A or Load-B and the participations from the remainder is more than ninety degrees for this study interval. In Figure 3.11 (b), the harmonic participation of Load-C is significantly higher compared to the rest of the network for the first thirty seconds of operation, and the current harmonics participation at the utility end rises from thirty seconds to sixty seconds. As shown in Figure 3.11 (b), the angle of phase among Load-C and the remainder of the network is below ninety degrees, leading to a greater total observed current with harmonics magnitude for Load-C as well as other loads.

3. Figures 3.7 (c) and (d) show that the Load-A produced 5^{th} and 7^{th} current harmonics are extremely close to the total 5^{th} and 7^{th} current harmonics measured at MP_1. Load-A appears to contribute substantially more harmonic current than the remainder of the network.

4. As demonstrated in Figure 3.9 (c), the harmonic participations of Load-B and the utility end are cumulative and introduce about equal amounts of current harmonics for the 5^{th} harmonics. Furthermore, Figure 3.9 (d) shows that Load-B's harmonic participation to the 7^{th} current harmonics is bigger compared to that of the remainder of the network. The angle of phase between Load-B and the rest of the network is computed to be less than 90 degrees, resulting in an increase in harmonic participations for 7^{th} current harmonics observed at MP_2.

5. Based on the data in Figure 3.11 (c) and (d), we can deduce that Load-C is accountable for a significant portion of the 5th as well 7th current harmonics located at MP_3. The remainder of the network's harmonic participation seems minor in compared to Load-C, and their contribution is just additive in terms of the total measured current harmonics at both the 5th and 7th harmonic levels.

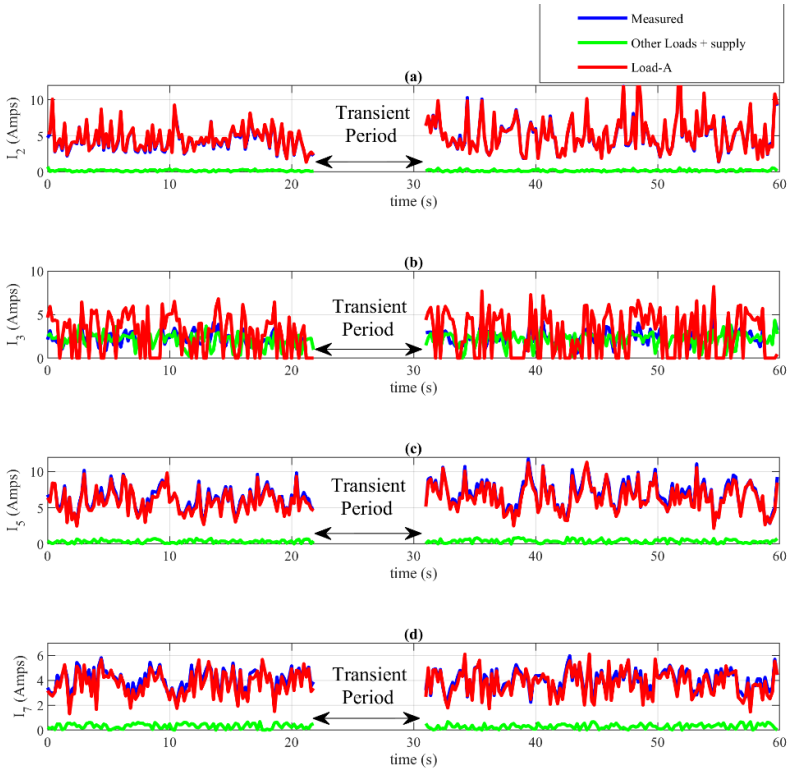

Figure 3.7. Load-A, remaining loads and the utility-end contributions to the current harmonics observed at MP1 for the harmonic orders: (a) 100 Hz (I_2), (b) 150 Hz (I_3), (c) 250 Hz (I_5) and (d) 350 Hz (I_7), calculated based on field measurements.

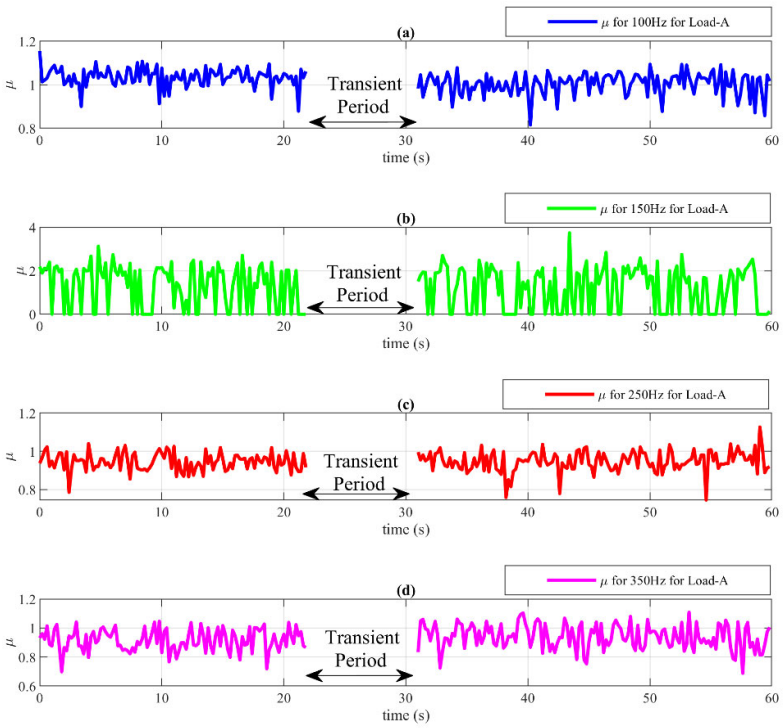

Figure 3.8. Distortion ratio findings across Load-A at MP1 with respect to the harmonic orders: (a) 100 Hz (I_2), (b) 150 Hz (I_3), (c) 250 Hz (I_5) and (d) 350 Hz (I_7) estimated from field measurements.

The distortion ratios (μ) for Load-A, Load-B, and Load-C are determined to validate the harmonic participations of the corresponding loads for the examined harmonic orders (Figures 3.8, 3.10, and 3.12). The conclusions that follow may be taken from these findings.

1. Figures 3.8 (a), 3.10 (a), and 3.12 (a) illustrate the distortion ratio computations for the second harmonic order for Load-A, Load-B, and Load-C, correspondingly. The distortion ratio results for Load-A as well as Load-C are almost identical to one, indicating that the demand-side participation is nearly equal to the total amount of current harmonics found for the second harmonics. The distortion rate of Load-B ranges across 0 and 1 in the fortieth and sixty-second intervals due to the enhanced utility side harmonic effect, whereas it is near to one in the first forty seconds.

2. The distortion ratio for the third harmonic order of Load-A along with Load-B is shown in Figures 3.8 (b) and 3.10 (b), respectively. The distortion rate for Load-A varies between zero and two due to phase removal between the load end with utility end current harmonic participations. For Load-B, the distortion rate varies between zero and four, indicating the fact that the utility end having a significant participation over the 3rd harmonics.

3. Figure 3.12 (b) indicates that for the initial forty seconds, the distortion ratio for the third harmonic order is near to 1 for Load-C, indicating that Load-C is the primary contributor to the third harmonic. From 40 to 60 seconds, the distortion rate ranges among 0 and 1, indicating that both Load-C and upward end demands are responsible for the harmonics participation.

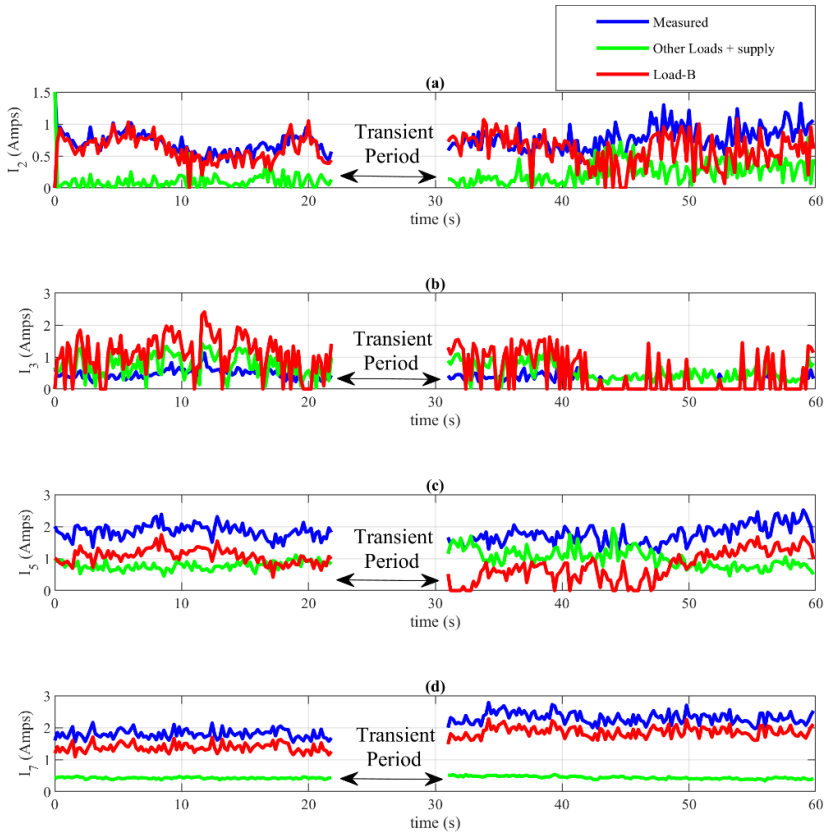

Figure 3.9. Load-B, remaining loads, and the utility-end contributions to the current harmonics observed at MP_2 for the harmonic orders: (a) 100 Hz (I_2), (b) 150 Hz (I_3), (c) 250 Hz (I_5), and (d) 350 Hz (I_7), calculated based on field measurements.

4. In Figure 3.8 (c) and (d), the distortion ratio for both the 5^{th} and 7^{th} harmonic orders are between 0.8 and 1. This shows that Load-A is the principal source of the harmonic current observed at MP_1's 5^{th} and 7^{th} harmonics.

5. When Load-B's harmonic participation is greater than the supply side, the distortion ratio falls between 0.4 and 0.6 during the first twenty seconds of operation, as shown in Figure 3.10 (c). The harmonic influence of the utility side outweighs that of the demand side between the thirtyth and fifty-first seconds, resulting in a decrease in Load-B's distortion ratio, which varies between 0 and 0.5. In the fiftieth and sixtieth second intervals, the harmonic participation of Load-B is stronger compared to the upstream end, causing the distortion rate to grow from 0.4 to 0.6. The distortion rate figure in Figure 3.10 (c) depicts the influence of the upstream side's harmonic current participation on the current data at MP_2.

6. Figure 3.10 (d) depicts the distortion ratio of Load-B for its seventh harmonic order, which varies between 0.75 - 0.8 for the first twenty seconds of operation and 0.75 - 0.9 for the final thirty seconds, indicating that the Load-B's harmonic participation is greater than the upstream side's. The distortion rate increases in the final thirty seconds compared to the first twenty, indicating an increase in the Load-B harmonic current participation.

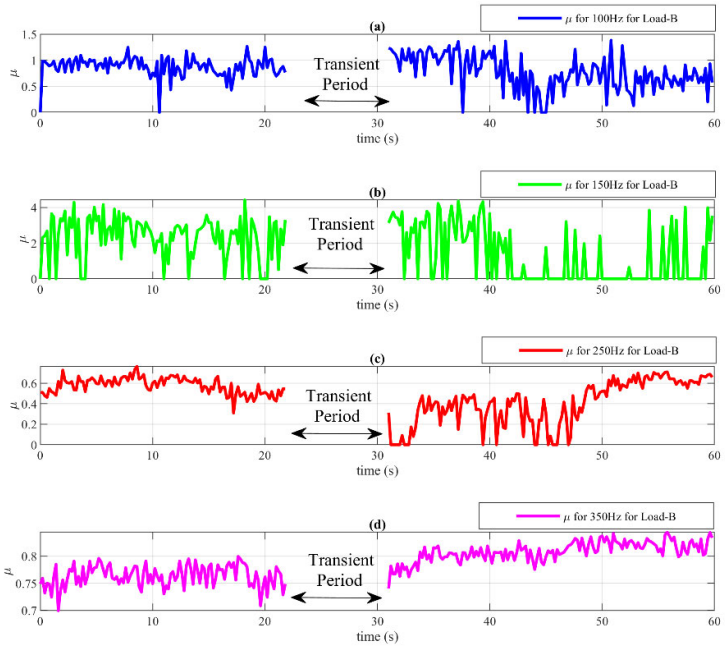

Figure 3.10. Distortion ratio findings across Load-B at MP_2 with respect to the harmonic orders: (a) 100 Hz (I_2), (b) 150 Hz (I_3), (c) 250 Hz (I_5), and (d) 350 Hz (I_7), estimated from field measurements.

7. The principal source of fifth- and seventh-harmonic flows detected in MP_3 is Load-C. In Figure 3.12 (c), the distortion ratio for the 5^{th} harmonic frequency runs from 0.9 up to 1.1, and in Figure 3.12 (d), it fluctuates among 0.85 up to 1.1, demonstrating that Load-C is mainly accountable for contributing to these harmonics.

The results of the harmonic contribution assessment are in agreement with the results of a previous study [11] using the same dataset. The approach described in this work, on the other hand, eliminates the requirement to compute upstream and demand side impedance within the PCC using current and voltage measurements. The suggested method successfully detects the harmonic participation of each facility and the supply side for each harmonic order. Additionally, the distortion ratio (μ) data are supplied to assist the harmonic contribution assessment.

3.4.2. Results from ERDEMİR transformer substation

Identification of harmonic impacts from I&S facilities and supply side

This chapter explains how the suggested algorithm is applied to real-time data obtained from the ERDEMİR transformer and a facility that gets electricity from a 13.8-kV-50-Hz transmission network. Figure 3.13 shows a simplified representation of the I&S plant's monitoring sites. Harmonic currents are time-synchronized and monitored inside facility on the SVC unit's shunt harmonic filter to determine the harmonic current accountability of both the upstream section and the EAF facility.

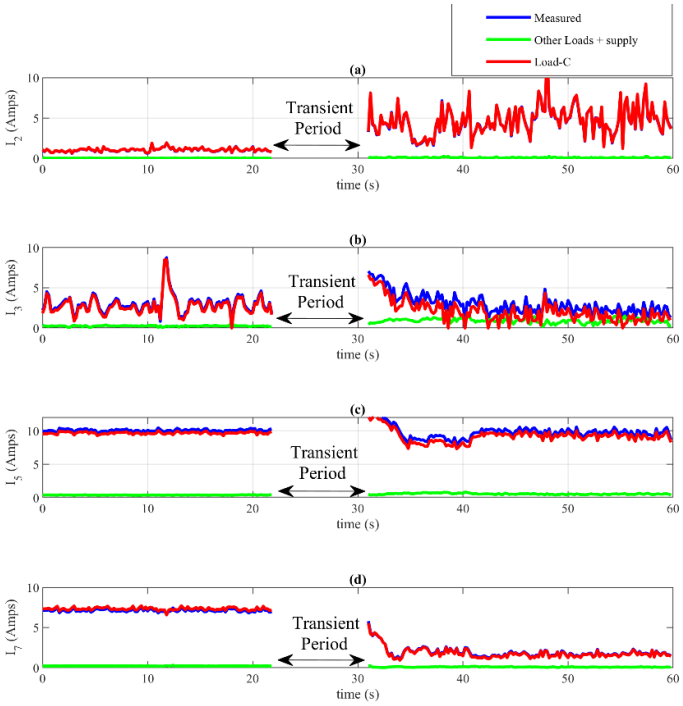

Figure 3.11. Load-C, remaining loads, and the utility-end contributions to the current harmonics observed at MP_3 for the harmonic orders: (a) 100 Hz (I_2), (b) 150 Hz (I_3), (c) 250 Hz (I_5), and (d) 350 Hz (I_7), calculated based on field measurements.

On-site, there are two ladle furnace plants with a capacity of 20 MVA. SVC also comes with a TCR of 32 MVAr and a 2nd harmonic filter of 14.2 MVAr of Type-C. PQ+ analyzers with a sample frequency of 25.6 kHz are used to gather data [18]. Due to the varying switching angles and unbalanced operational states of the thyristors, TCR systems exhibit nonlinear characteristics, resulting in the generation of harmonics at frequency multiples of the nominal frequency. To address this issue, the SVC system includes a second harmonic filter that filters out harmonics generated by both the TCR mechanism as well as the ladle furnaces.

As shown in Figure 3.13, the suggested approach for detecting harmonic accountability is used to examine the participations of the upstream side and the facility to the second, third, fifth, and seventh current harmonics observed at MP_1. Figure 3.14 depicts the findings of this investigation, which may be stated as follows:

1. As illustrated in Figure 3.14 (a), the load side produces a considerable share of the second current harmonics recorded at the PCC.

2. According to Figure 3.14 (c), the fifth current harmonic receives an important portion from the electricity supply side. The overall observed magnitude of the fifth harmonic current, nevertheless, is less than the sum of the facility side and utility side contributions, most likely due to a phase cancellation effect between the two contributions.

3. As shown in Figures 3.14 (b) and (d), the facility side's participation to the third and seventh harmonics of the current is almost equivalent to the total estimated harmonic current. Furthermore, the upstream side participation to those harmonic frequencies is insignificant.

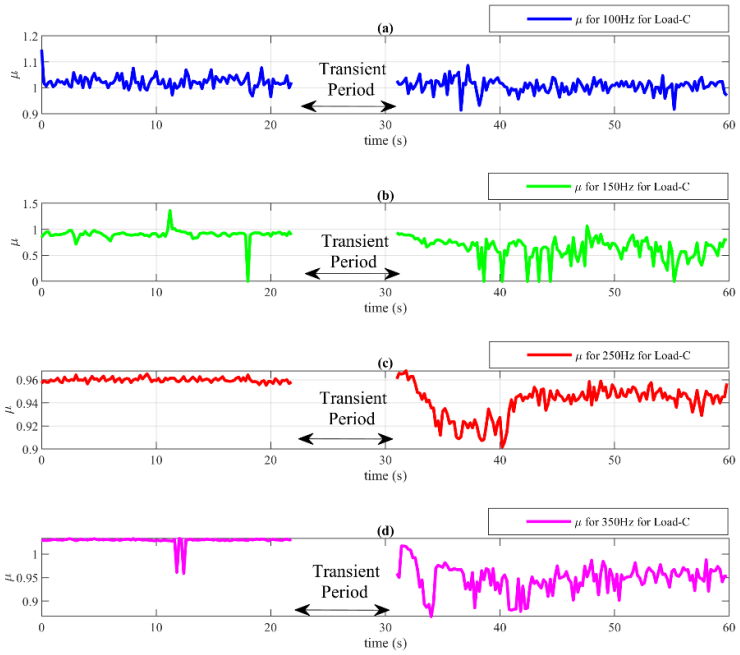

Figure 3.12. Distortion ratio findings across Load-C at MP_3 with respect to the harmonic orders: (a) 100 Hz (I_2), (b) 150 Hz (I_3), (c) 250 Hz (I_5), and (d) 350 Hz (I_7), estimated from field measurements.

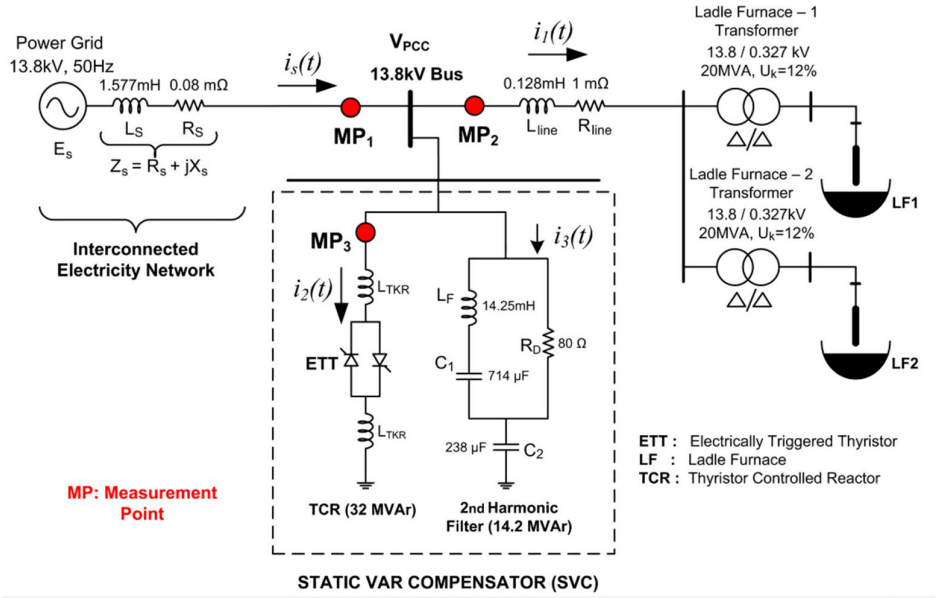

Figure 3.13. ERDEMİR transformer substation single line diagram that depicts the ladle furnace facilities, SVC structure, and measuring points [11].

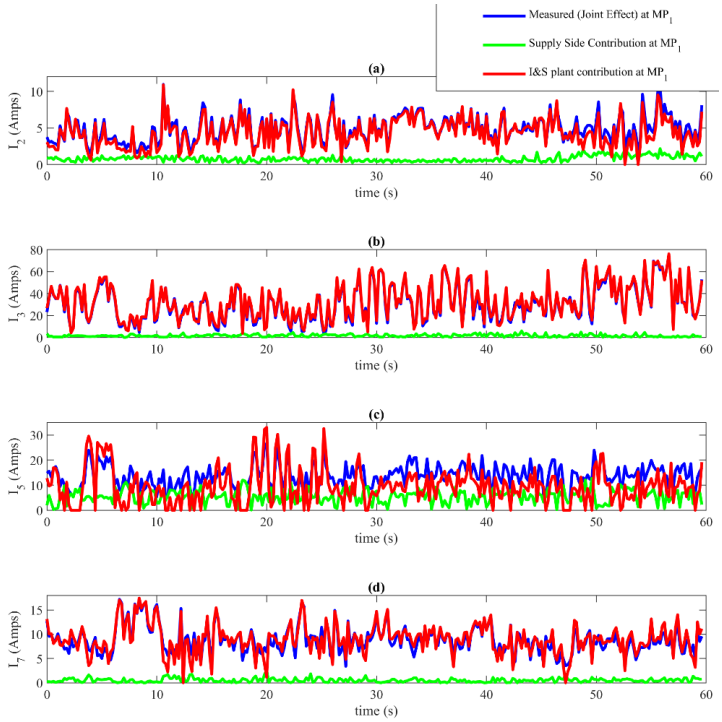

Figure 3.14. I&S plant and utility-side contributions to the current harmonics observed at MP_1 for the harmonic orders: (a) 100 Hz (I_2), (b) 150 Hz (I_3), (c) 250 Hz (I_5) and (d) 350 Hz (I_7), calculated based on field measurements.

The waveform correlation evaluation results are consistent with those published in prior research [11]. The current study determined the harmonic current participations of both the upstream and demand sides without the need for real-time calculation of source and load impedances. The next section delves into an in-depth assessment of the utility and facility ends' harmonic current participations in relation to the I&S facility's shunt harmonic filter.

Identification of harmonic current accountability on the ERDEMİR I&S plant's shunt harmonic filter

The second harmonic currents generated by the demands are filtered out by the harmonic filter located in ERDEMIR plant seen in Figure 3.13. By incorporating the data from the prior chapter into the mathematical model described below, we will offer the upstream and demand side current harmonics filtered through the facility's harmonic filter in this chapter.

Figure 3.15 (a) and (b) [12] demonstrate Norton's equivalent circuit models being used to represent both the utility and demand side current participations to the harmonic filter of the ERDEMIR plant.

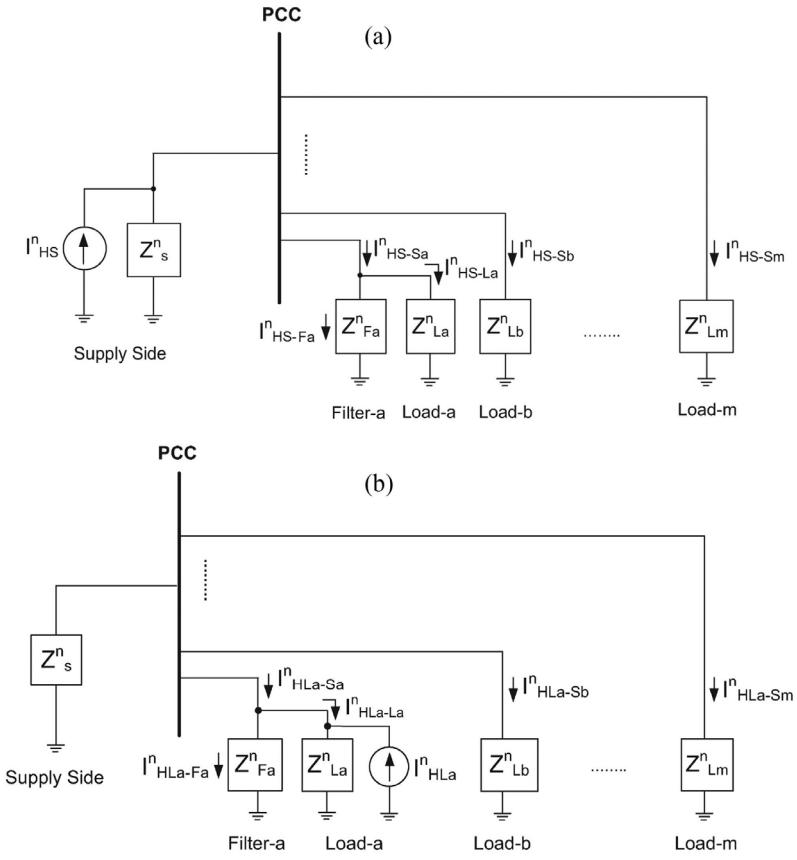

Figure 3.15. Harmonic behavior of the network at ERDEMİR I&S plant is represented using the single-phase Norton equal circuit diagram. Subfigure (a) shows the model when only the supply-side current source (I^n_{HS}) is active, while subfigure (b) shows the model when only the load-side current source (I^n_{HLa}) is active [12].

Figure 3.15 (a) depicts Norton's equal circuit architecture for upstream part current participation to Load-a and Filter-a with all current sources except I_{HS}^{n} inactive. $I_{HS\text{-}Sa}^{n}$ represents the upstream part harmonic current participation in Load-a and Filter-a, whereas $I_{HS\text{-}La}^{n}$ represents the upstream part harmonic current participation in Load-a. The phase difference between these signals demonstrates the participation of the upstream part harmonic current $I_{HS\text{-}Fa}^{n}$ on the Load-a's harmonic filter, as indicated in Equation 3.12.

Similarly, when the facility part current source I_{HLa}^{n} is isolated, $I_{HLa\text{-}Sa}^{n}$ indicates the harmonic current participation from the upstream part to Load-a and Filter-a, while $I_{HLa\text{-}La}^{n}$ represents the harmonic current participation from Load-a its own, as illustrated in Figure 3.15 (b). Load-A's harmonic current participation to its harmonic filter ($I_{HLa\text{-}Fa}^{n}$) is determined by Equation 3.13 as the phase variation among $I_{HLa\text{-}Sa}^{n}$ and $I_{HLa\text{-}La}^{n}$.

$$I_{\text{HS-Fa}}^{n} = I_{\text{HS-Sa}}^{n} - I_{\text{HS-La}}^{n} \tag{3.12}$$

$$I_{\text{HLa-Fa}}^{n} = I_{\text{HLa-Sa}}^{n} - I_{\text{HLa-La}}^{n} \tag{3.13}$$

The utility side's harmonic current participations are represented by $I_{HS\text{-}Sb}^{n}$ and $I_{HS\text{-}Sm}^{n}$, whereas Load-a participations onto Load-b as well as Load-m are represented by $I_{HLa\text{-}Sb}^{n}$ and $I_{HLa\text{-}Sm}^{n}$, respectively. For both models shown in Figure 3.15, measurements inside the plant are considered to be obtained exclusively at Load-a.

In [12], the upstream, filter and facility side impedance values (Z_{s}^{n}, Z_{Fa}^{n}, Z_{La}^{n}, Z_{Lb}^{n},...., Z_{Lm}^{n}) are obtained for every ten-period data frame to determine the harmonic accountability of the upstream and demand side on the harmonic filter of the iron-steel facility.

As illustrated in Figure 3.15, the proposed technique employs waveform correlation evaluation to detect harmonic contribution for each data measurement point (MP_1, MP_2, MP_3) and to compute the phase and magnitude quantities for every single current component for each harmonic frequency. The harmonic current generated by the facility side and upstream side on the I&S plant's harmonic filter is then calculated using Equations 3.12 and 3.13. The outcomes of this approach are shown in Figures 3.16 and 3.17 for the 2nd, 3rd, 5th, and 7th harmonics, and the 4th, 9th, 11th, and 13th harmonics.

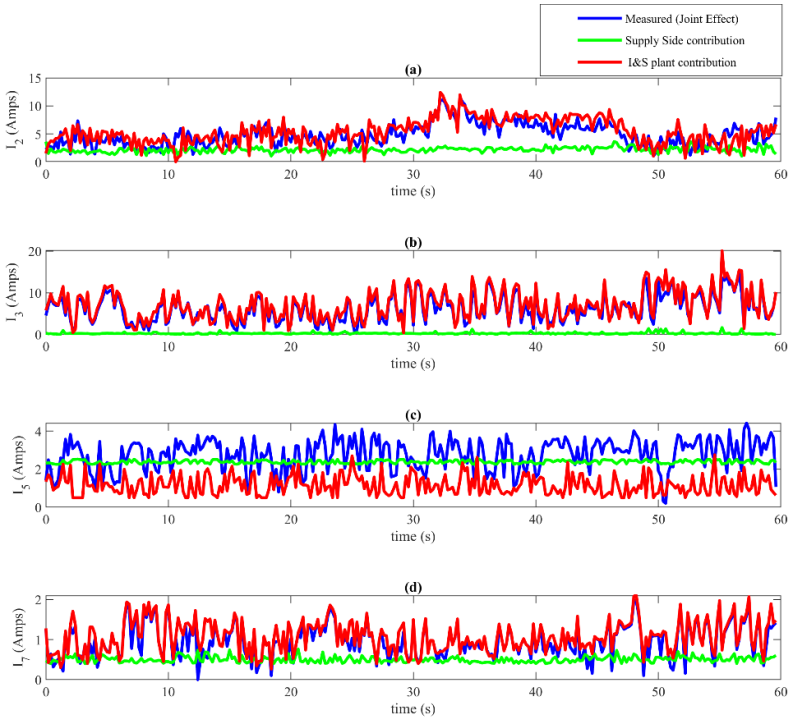

Figure 3.16. I&S plant and utility-side contributions to current harmonics recorded at the iron and steel plant's harmonic filter for the harmonic orders: (a) 100 Hz (I_2), (b) 150 Hz (I_3), (c) 250 Hz (I_5), and (d) 350 Hz (I_7), computed from field measurements.

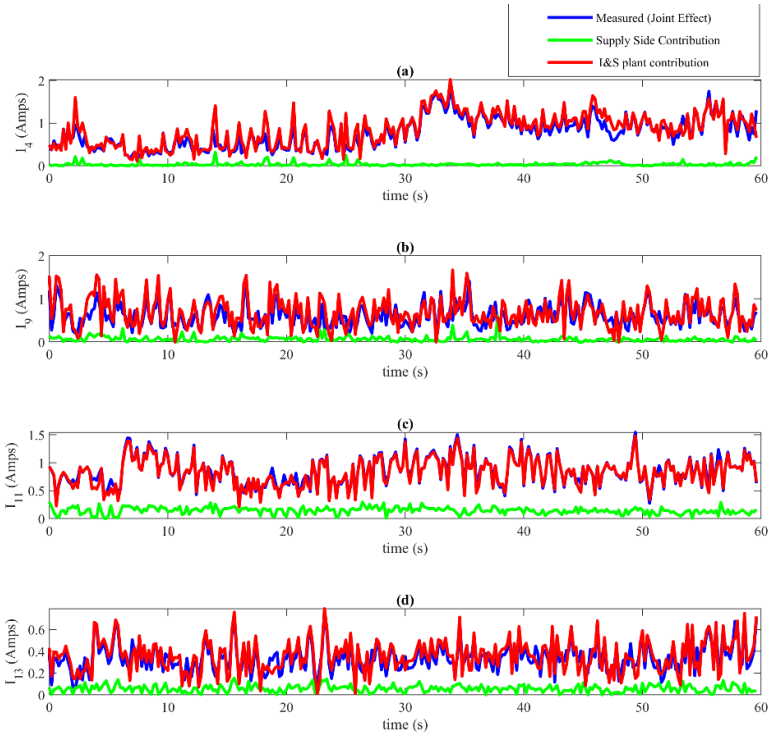

Figure 3.17. I&S plant and utility-side contributions to current harmonics recorded at the iron and steel plant's harmonic filter for the harmonic orders: (a) 200 Hz (I4), (b) 450 Hz (I9), (c) 550 Hz (I11), and (d) 650 Hz (I13), computed from field measurements.

The findings presented in Figures 3.16 and 3.17 can be summarized below:

1. As seen in Figure 3.16 (a), the demand side is responsible for a large portion of the second current harmonics found through the filter, which is roughly equivalent to the overall current of harmonics detected on the filter. The upstream side contributes 20% of the overall current at the second-harmonic order obtained throughout the filter.

2. The facility side is mostly responsible for the third current harmonics measured across the filter, as shown in Figure 3.16 (b). The supply side participation in the third harmonic order is minimal.

3. The I&S plant's harmonic filter significantly decreases the fifth current harmonics from the upstream side, as seen in Figure 3.16 (c). The load side contributes far less to the fifth current harmonics than the utility side.

4. As demonstrated in Figure 3.16 (d), the amount of harmonic current delivered by the facility side is almost comparable with the total seventh current harmonics detected through the filter itself. Furthermore, the shunt harmonic filter efficiently filters the majority of the upstream side seventh harmonics.

5. For the 4^{th}, 9^{th}, 11^{th}, and 13^{th} harmonics, according to Figure 3.17, the harmonic participation on the facility side is roughly equivalent to the total measured current harmonics through the harmonic filter. The source side's participation is far smaller than the facility. The suggested approach can calculate the harmonic current participation at higher-level frequencies. As seen in Figure 3.17, the amplitude of the harmonic impact diminishes with increasing frequency level. Consequently, this study focuses on frequencies with greater harmonic contribution.

The difference between the calculated 5^{th} and 7^{th} current harmonics on the I&S plant's second-order filter and the harmonic current produced by the facility side is due to the filter absorbing a substantial amount of the upstream side's fifth current harmonics and a specific level of seventh current harmonics. The findings obtained using the waveform correlation technique shown in Figure 3.16 are similar with the results obtained using the impedance computation predicated approach described with [12] to estimate the supply and facility side current participation on the harmonic filter of the iron and steel plant.

4. DERIVING THE MATHEMATICAL RELATIONSHIP BETWEEN VOLTAGE & CURRENT WAVEFORM CORRELATION AND AMOUNT OF HARMONIC VOLTAGE CONTRIBUTION AT A PCC

This chapter describes a novel method for assessing the harmonic voltage participations of EAF facilities powered by the PCC. The approach depends on the correlation of the waveforms of the voltage at the PCC and feeder currents. It employs a developed relationship among the correlation coefficient and each plant's harmonic voltage participation. The essential premise is that harmonic voltage at the PCC is created by a combination of voltage dips on the source side impedance induced by separate feeder currents.

This approach offers various advantages. It does not necessitate calculating client-side impedance and has a modest computational overhead when compared to other techniques. Second, unlike previous techniques such as [11] and [12], just the associated feeder current is required to assess the participation of one plant. This makes it more efficient and easier to use.

The proposed approach has been validated using PSCAD software using a simulation model that includes the presence of harmonic loads in the PCC and on the supply side. Also, the approach has been applied to measurement datasets read from multiple electrical substations serving multiple EAF facilities. The findings showed that the proposed method is successful in detecting harmonic voltage contribution in PCC.

The proposed approach has been improved to demonstrate the influence of the EAF plants' compensating mechanisms. This is accomplished by doing extra correlation computations between feeder currents and inside facility current readings to discover harmonic current dropping in an affected plant with a robust compensating mechanism.

This section provides the mathematical link between the current and voltage waveform relationships and the degree of harmonic voltage participation at a PCC.

The technique is validated in Chapter 5 using PSCAD and MATLAB in simulations. The approach has also been applied to real time field data observations at a PCC that feeds EAFs, and outcomes are presented.

Using different examples, Chapter 6 simulates the upstream and facility side accountability for the harmonic current on an affected plant's shunt harmonic filter. The suggested approach is utilized to validate situations of sufferer plants that have powerful harmonic compensators.

4.1. A Mathematical Derivation of the Suggested Technique for Identifying Harmonic Voltage Accountability at PCC

Figure 4.1 shows a simplified schematic of a PCC that supplies n plants. The upstream side line impedance and voltage are indicated via R_s+jX_s and Es, respectively. Es is intended to stay constant at the nominal grid voltage magnitude for varying load levels at the nominal frequency in a robust electrical network that feeds the PCC. At other frequencies, such as harmonic and interharmonic orders, Es may have a small magnitude and change over time due to harmonic participations from upstream sides.

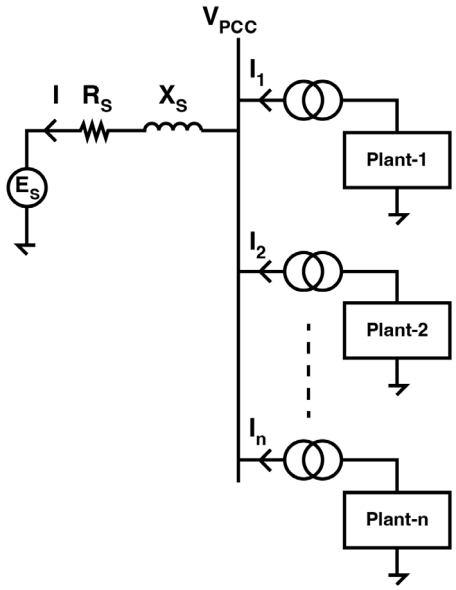

Figure 4.1. A visual depiction of a PCC that supplies n feeders.

Voltage phasor at PCC for any frequency order may be proved using Equation 4.1 and in Figure 4.2.

$$\mathbf{V_{PCC}} = E_{\mathbf{s}} + \mathbf{I}\left(R_s + jX_s\right) \tag{4.1}$$

I is the sum of each of the feeder currents, while R_S+jX_S represents the utility side line impedance. The amount may be collected from the power supply authorities during a certain period on the electrical network, or alternatively it can be calculated if adequate data is available on the network [34].

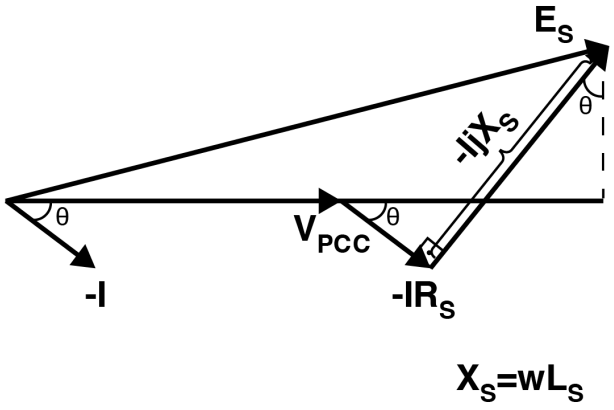

Figure 4.2. A phasor representation for the nominal frequency with a significant and nearly stable Es for a robust electrical network.

$I = I_1 + I_2 + ... + I_n$ is the upstream side current, while n is the entire number of feeders across the PCC. Equation 4.2 may be used to explain V_{PCC}.

$$\mathbf{V_{PCC}} = E_{\mathbf{s}} + I_{\mathbf{1}}(R_s + jX_s) + I_{\mathbf{2}}(R_s + jX_s) + \cdots + I_{\mathbf{n}}(R_s + jX_s) \quad (4.2)$$

Equation 4.2 describes the PCC voltage, where each term in the summation represents the contribution of each harmonic and interharmonic component. E_s denotes the utility's standard voltage at the nominal frequency, while for harmonics and interharmonics, it denotes the source side harmonic contribution. E_s can have a variable value for harmonics and interharmonics according to the situation of the grid's top side, and it can even be zero. E_s must have an amplitude that is similar to the harmonic participations of the demand feeders.

As illustrated in Figure 4.3, the total voltage phasor across the PCC for a particular harmonic order may be determined by adding the voltage phasors for each individual feeder with the utility side.

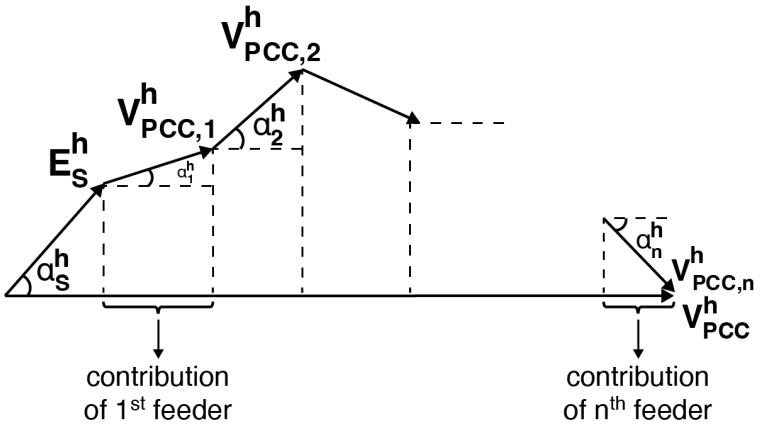

Figure 4.3. The supply side and feeder contributions to the voltage at the PCC at the h^{th} harmonic order.

The angle α_n^h in Figure 4.3 reflects the phase difference that exists between the h^{th} harmonic order auxiliary voltage phasor of the n^{th} feeder and the voltage at the PCC in the n^{th} harmonic order. As a result, Equation 4.3 shows the participation of the n^{th} feeder.

$$V_{C,n}^h = | V_{\mathbf{PCC},n}^{\mathbf{h}} | \cos\left(\alpha_n^h\right) \tag{4.3}$$

The relative harmonic accountability of the n^{th} feeder may be calculated using Equation 4.4.

$$H_{\mathrm{PCC},n}^h = \frac{V_{C,n}^h}{| V_{\mathbf{PCC}}^{\mathbf{h}} |} \times 100\% \tag{4.4}$$

Figure 4.4 demonstrates the relationship between the harmonic participation angle α, which represents the phase difference between the PCC voltage and the contributing voltages, along with the angle θ, that represents the phase difference between each feeder current and the voltage at PCC.

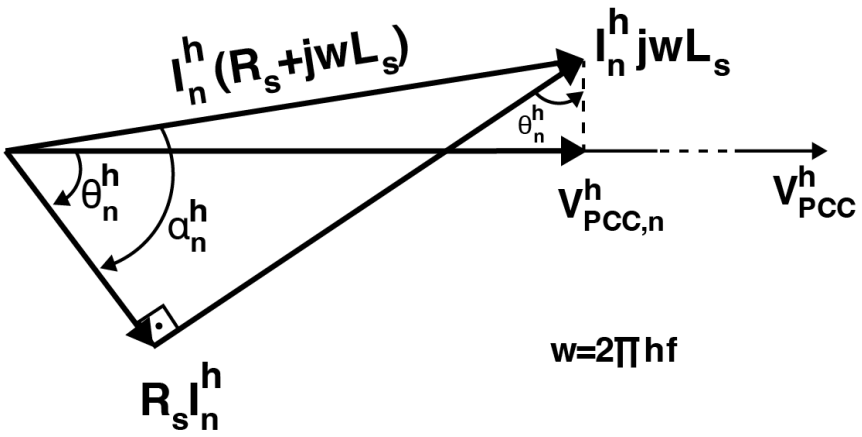

Figure 4.4. The phasor depiction of the n[th] feeder voltage contributing at the h[th] harmonic as well as the n[th] feeder current I_n^h.

While θ may be measured using feeder currents and PCC voltage, measuring α directly isn't possible. In Figure 4.4, θ_n^h represents the angle that is formed by the n[th] feeder current and PCC voltage at the h^{th} harmonic order. The angle among the phasor of the harmonic voltage generated via the n[th] current at feeder and the phasor of the feeder current I_n^h, on the other hand, is denoted by α_n^h. Thus, using Equation 4.5, one can calculate the participation caused by the n[th] current at feeder on the PCC voltage at the h^{th} harmonic order.

$$V_{PCC,n}^h = \mathbf{I_n^h}\left(R_s + j\omega L_s\right)\cos\left(\alpha_n^h - \theta_n^h\right) \tag{4.5}$$

Given that measurements of V_{PCC} and I_n^h are obtainable, determining the angle between them is a straightforward process that involves estimating the correlation coefficient among their respective sampled values. The correlation coefficient of just two recorded signals, x_k and y_k, may be calculated using Equation 4.6.

$$r = \frac{\sum_{n=1}^{N} x_k y_k}{\sqrt{\sum_{n=1}^{N} x_k^2}\sqrt{\sum_{n=1}^{N} y_k^2}} \tag{4.6}$$

In the time space, Equations 4.7 and 4.8 determine the signals of the n[th] harmonic elements of the voltage at PCC and the n[th] current at feeder.

$$V_{\mathrm{PCC}}^{h}(t) = \mid V_{\mathbf{PCC}}^{\mathbf{h}} \mid \sin(h\omega t) \tag{4.7}$$

$$I_{\mathrm{PCC},n}^{h}(t) = \mid I_{\mathbf{PCC},n}^{\mathbf{h}} \mid \sin\left(h\omega t + \theta_n^h\right) \tag{4.8}$$

Equations 4.9 and 4.10 provide the sampled forms of these waveforms.

$$x_k = \mid \mathbf{V}_{\mathbf{PCC}}^{\mathbf{h}} \mid \sin\left[\frac{2\pi h(k-1)}{N}\right] \tag{4.9}$$

$$y_k = \mid \mathbf{I}_{\mathbf{PCC},n}^{\mathbf{h}} \mid \sin\left[\frac{2\pi h(k-1)}{N} + \theta_n^h\right] \tag{4.10}$$

With the assumption that the duration of sampling is a whole-number multiple of the current or voltage signal duration, Equations 4.11, 4.12, and 4.13 may be used to reduce the denominator and numerator components of r, making them independent of k.

$$x_k y_k = \mid \mathbf{V}_{\mathbf{PCC}}^{h} \mid\mid \mathbf{I}_{\mathbf{PCC},n}^{\mathbf{h}} \mid \cos\left(\theta_n^h\right) \tag{4.11}$$

$$x_k^{\,2} = \mid \mathbf{V}_{\mathbf{PCC}}^{\mathbf{h}} \mid^2 \tag{4.12}$$

$$y_k^{\,2} = \mid \mathbf{I}_{\mathbf{PCC},n}^{\mathbf{h}} \mid^2 \tag{4.13}$$

As a result, Equation 4.14 provides the form that r takes, with N representing the analysis window size in samples.

$$r = \frac{\sum_{n=1}^{N} \mid \mathbf{V}_{\mathbf{PCC}}^{\mathbf{h}} \mid\mid \mathbf{I}_{\mathbf{PCC},n}^{\mathbf{h}} \mid \cos(\theta_n^h)}{\sqrt{\sum_{n=1}^{N} \mid \mathbf{V}_{\mathbf{PCC}}^{\mathbf{h}} \mid^2} \sqrt{\sum_{n=1}^{N} \mid \mathbf{I}_{\mathbf{PCC},n}^{\mathbf{h}} \mid^2}} \tag{4.14}$$

Due to the independence of all the summation arguments with respect to k, Equation 4.14 can be simplified to equation 4.15.

$$r=\cos\left(\theta_n^h\right) \tag{4.15}$$

In the scenario where R_s is much smaller than wL_s which is illustrated in Figure 4.5 and can occur for certain harmonic orders, Equation 4.5 can be reconfigured using the correlation coefficient and expressed through Equations 4.16 to 4.18.

$$V_{\mathrm{PCC},n}^h \cong \left| I_n^h \left(R_s + j\omega L_s\right)\right| \sin\left(\theta_n^h\right) \tag{4.16}$$

$$V_{\mathrm{PCC},n}^h = \left| I_n^h \right| \sqrt{R_s^2 + (\omega L_s)^2}\sqrt{1-\cos(\theta_n^h)^2} \tag{4.17}$$

$$V_{\mathrm{PCC},n}^h = \left| I_n^h \right| \sqrt{R_s^2 + (\omega L_s)^2}\sqrt{1-r^2} \tag{4.18}$$

After obtaining the correlation coefficient among the voltage at PCC and the feeder current, Equation 4.18 may be used to determine the participation of the current at the n^{th} feeder on the h^{th} harmonic of the PCC voltage.

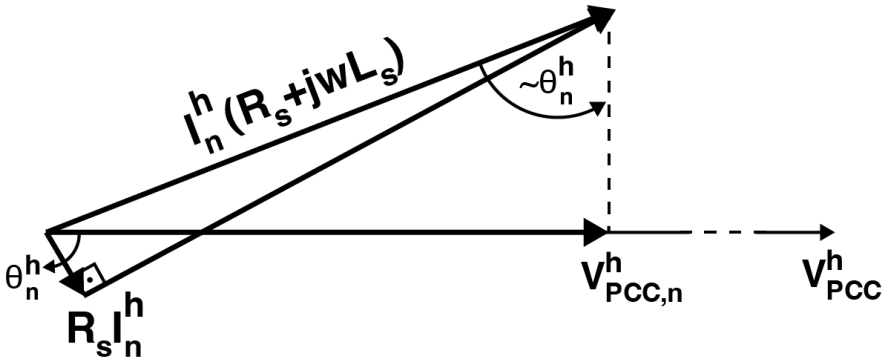

Figure 4.5. The phasor representation of the nth feeder's voltage contribution at the h^{th} harmonic frequency, as well as the current at nth feeder I_n^h where Rs is much less than wL.

5. WAVEFORM CORRELATION BASED VOLTAGE HARMONIC CONTRIBUTION DETECTION AT A PCC

5.1. The Proposed Method's Validation in Simulation Environment

The suggested technique is validated using a network model in the PSCAD software that simulates the existence of harmonics producing demands as well as the supply side at the PCC. Then, simulation data is processed in MATLAB to apply the method and evaluate its performance using the results. Figure 5.1 depicts the efficacy of the suggested technique by simulating three harmonic-generating demands (Load-A with 5th harmonic filter) and a utility side harmonic source with distortions.

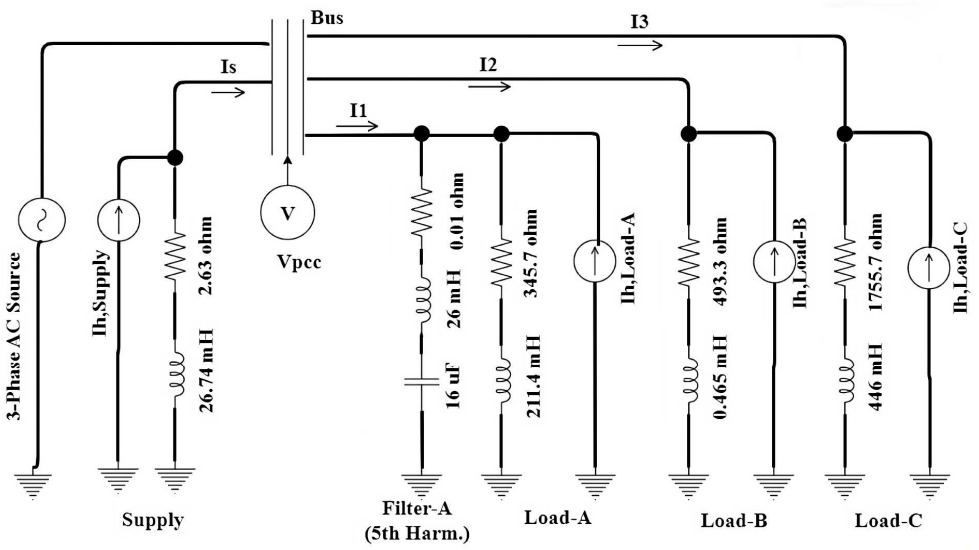

Figure 5.1. Three-phase system design for testing the correctness of the proposed technique.

Following the computer simulation investigation, the gathered data is used to determine the current harmonic magnitudes of the demand and utility sides, along with the harmonic voltage participation at the PCC. To restrict the passage of Load-A's fifth order harmonic current toward the source side, a fifth order harmonic filter is installed at Load-A's PCC with the network, as illustrated in Figure 5.1.

The proposed method is confirmed through the following steps.

1. Table 5.1 lists the magnitudes of the harmonic currents used as inputs for the circuit diagram shown in Figure 5.1. Without sacrificing generalization, the phase angles of the harmonic currents $I_{h,\text{Load-A}}$, $I_{h,\text{Load-B}}$, $I_{h,\text{Load-C}}$ and, $I_{h,\text{Supply}}$ are set to zero. The default source voltage Vpcc has been configured as 13.8 kV, while the system's default nominal frequency is adjusted to 50 Hz. The experimental dataset is generated for sixty seconds at a sampling frequency of 4 kHz.

Table 5.1. PSCAD simulation input parameters f: Harmonic Frequency (Hz), I: Current Harmonics RMS Amplitude (Ampere)

Frequency (Hz)	$I_{h,\text{Supply}}$	$I_{h,\text{Load-A}}$	$I_{h,\text{Load-B}}$	$I_{h,\text{Load-C}}$
100	30	-	-	-
150	50	-	100	-
250	80	50	-	-
350	100	-	-	150

2. The magnitude and phase spectra of the voltage and harmonic current generators are computed for each separate ten-period DFT frame utilizing the subgroup computation approach of IEC-61000-4-7. Table 5.2 summarizes the findings.

Table 5.2. The recorded voltage and current signals' DFT amplitude spectra. f: Harmonic Frequency (Hz), V: PCC Voltage DFT Amplitude for each harmonic order (Volt), I: PCC Current DFT Amplitude for each harmonic order (Ampere)

Frequency (Hz)	V_{pcc}(V)	$I_{h,\text{supply}}$(A)	$I_{h,\text{Load-A}}$ (A)	$I_{h,\text{Load-B}}$ (A)	$I_{h,\text{Load-C}}$ (A)
100 Hz	1702.35	46.54	18.36	17.83	11.53
150 Hz	411.72	75.33	9.43	46.65	4.73
250 Hz	137.20	84.35	77.53	2.28	4.37
350 Hz	373.12	92.68	13.23	4.12	74.78

3. The method proposed in [25] calculates the harmonic current participation at the PCC using the DFT spectra of the current and voltage obtained in the preceding step.

4. The results of the harmonic current accountability performed using the proposed method are shown in Table 5.3 for both the utility and demand sides across the PCC, while the Table 5.4 shows the RMSE for the participation of current harmonic on both the utility and demand sides of the PCC for each harmonic frequency.

Table 5.3. Harmonic Current Participation results associated with each harmonic order f: Harmonic Frequency, I: Harmonic Current RMS Amplitude

Frequency	$I_{h,supply}$ (A)	$I_{h,Load\text{-}A}$ (A)	$I_{h,Load\text{-}B}$ (A)	$I_{h,Load\text{-}C}$ (A)
100 Hz	31.36	-	-	-
150 Hz	51.08	-	98.7	-
250 Hz	77.55	48.4	-	-
350 Hz	98.24	-	-	147.76

5. The harmonic current contribution analysis results in Table 5.3 closely mirror the input quantities in Table 5.1. This relationship results in an exact determination of the harmonic current accountability in both the load and supply sections of the corresponding harmonic order. The findings of this study are then used to calculate harmonic voltage contributions on the utility and demand sides.

Table 5.4. The RMSE for the harmonic current contribution findings acquired in the PSCAD experiment using the suggested technique for each harmonic order.

Frequency (Hz)	$RMSE_{Supply}$	$RMSE_{Load\text{-}A}$	$RMSE_{Load\text{-}B}$	$RMSE_{Load\text{-}C}$
100	0.0267	-	-	-
150	0.0923	-	0.0768	-
250	0.0634	0.0823	-	-
350	0.0821	-	-	0.0934

6. Table 5.5. shows the harmonic voltage contribution at the PCC for each harmonic order using the formulae provided in Equations (4.9) through (4.18).

Table 5.5. Harmonic Voltage Contribution results associated with each harmonic order f: Harmonic Frequency (Hz), I: Harmonic Voltage RMS Amplitude (Volt)

Frequency (Hz)	$V_{h,Supply}$	$V_{h,Load\text{-}A}$	$V_{h,Load\text{-}B}$	$V_{h,Load\text{-}C}$
100	12.43	-	-	-
150	23.85	-	89.17	-
250	55.72	18.11	-	-
350	83.75	-	-	114.56

7. The efficacy of the proposed method is emphasized by contrasting it with the accuracy of the technique presented in [11]. The evaluation is centered on the RMSE for the harmonic voltage contribution, and the findings are shown in Tables 5.6 and 5.7 for each harmonic order.

Table 5.6. The RMSE for the harmonic voltage contribution findings acquired in the PSCAD experiment using the suggested technique for each harmonic order.

Frequency (Hz)	$RMSE_{supply}$	$RMSE_{Load-A}$	$RMSE_{Load-B}$	$RMSE_{Load-C}$
100	0.0240	-	-	-
150	0.0230	-	0.0840	-
250	0.0470	0.0130	-	-
350	0.0530	-	-	0.0790

8. The proposed technique, however, differs from the method employed in [11] in that it doesn't depend on circuitry modeling for identifying the harmonic participation of the utility and demand sides. The approach, on the other hand, uses waveform correlation algorithms to calculate harmonic voltage accountability based on observed current and voltage data. Regardless of these variations, the RMSE outcomes for both techniques are similar, and the suggested strategy is shown to be successful.

Table 5.7. The RMSE for the harmonic voltage contribution findings acquired in the PSCAD experiment using the approach given in [11] for each harmonic order.

Frequency (Hz)	$RMSE_{Supply}$	$RMSE_{Load-A}$	$RMSE_{Load-B}$	$RMSE_{Load-C}$
100	0.0072	-	-	-
150	0.0047	-	0.0051	-
250	0.0082	0.0062	-	-
350	0.0091	-	-	0.0024

9. The results of the harmonic voltage and current participation study show that the proposed method might be used in real-time PQ analysis to identify harmonics from both the demand and source sides. Because the suggested approach requires no impedance calculations, the possibility for speedier findings may outweigh the modest accuracy concern.

10. The approach has been validated in a simulation environment as illustrated in Figure 5.1 representing an initial step towards employing the methodology to measure real-time data from multiple substations as shown in Figure 3.6. In the following section, the approach will be utilized with real-time field data.

5.2. Application of the Suggested Technique to Real Measurement Data

The proposed approach for measuring harmonic voltage contribution is tested using data collected from ISKENDERUN transformer facility (ISK-2), that represents one of the PCCs of the Turkish Electricity Transmission Network, as shown within Figure 3.6. In-depth information on the schematic diagram and measurement points for data collection are discussed in Section 3.4.1.

The proposed approach for determining harmonic voltage responsibility is used to compute the voltage harmonic contributions of Loads A, B, and C for the 2^{nd}, 3^{rd}, 5^{th}, and 7^{th} harmonic frequencies and Figures 5.2, 5.3, 5.4, and 5.5 depict the results. The harmonic current and voltage participations of each load are shown individually in Figures 5.6, 5.7, and 5.8 for various harmonic orders. The study is not restricted to any particular harmonic or interharmonic frequency, although for EAF plants, the 2^{nd}, 3^{rd}, 5^{th}, and 7^{th} harmonics have the greatest magnitudes and hence are of main relevance in the research.

The behavior of an EAF is very complex and not easily predictable due to its highly dynamic and non-linear nature. Throughout the melting process, the arcing current and voltage characteristics fluctuate frequently, and arc initiation and suppression occur at random and unexpectedly, particularly in the early phases of the EAF process. Furthermore, the metal composition of the furnace changes from tap to tap, adding to the unpredictability of the harmonic elements fed through the electric power network via the EAF. When a spark forms over melted or half-melted metallic material, the EAF's control mechanism eliminates the carbon-based electrodes, leading to extremely volatile harmonic elements which are hard to precisely describe and anticipate.

Although the second harmonic is not typically associated with the transmission system, it is a common harmonic in EAF operation. This is due to the emergence of unanticipated sparks among processes across the metallic material within the oven and the controller's immediate reaction. As a result, in the context of EAF functioning, the 2nd harmonic becomes a major component.

The figures show the following results, which may be summarized:

1. Figure 5.2 shows that during the first twenty seconds, Load-A produces the bulk of the second voltage harmonic, however during the remaining thirty seconds, Load-A as well Load-C contribute much more harmonics than Load-B. Load-B has a substantially smaller second harmonic participation about ten times less than the other loads, which is not surprising given that Loads A and C are EAF plants and Load-B is an industrial rolling mill facility. The rationale for this conclusion is because the 2nd harmonic is a byproduct of the EAF operation's activity rather than a fundamental harmonic of the transmission network.

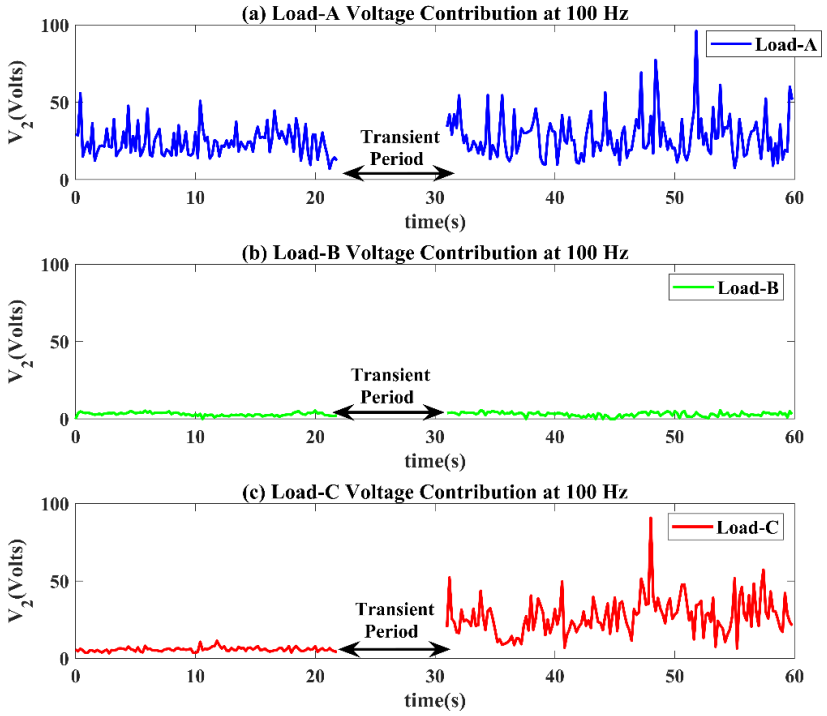

Figure 5.2. The contributions of Loads A, B, and C to the second order harmonic voltage observed at the PCC shown in Figure 3.6 are calculated and graphed in three ways: (a) depicts harmonic voltage participation of Load-A at 100 Hz (b) depicts harmonic voltage participation of Load-B at 100 Hz (c) depicts harmonic voltage participation of Load-C at 100 Hz, as calculated from field data.

2. Load-A contributes more to the third harmonic than Load-B together with Load-C at all intervals, as seen in Figure 5.3. The harmonic participation of Load-C to the voltage at the PCC is about half of Load-A's harmonic participation for the 3rd harmonic order. For this harmonic order, Load-B's harmonic participation increased and now accounts for roughly a fifth of Load-A's harmonic participation.

3. The fifth harmonic voltage participation of Load-C is the most significant of any load in the whole interval shown in Figure 5.4. In the initial 20 seconds, Load-C has twice the harmonic participation of Load-A, while during the last thirty seconds, Load-C's participation is nearly half of its starting value. Load-A's harmonic participation is almost constant across all intervals. Load-B contributes around ten times less to the fifth harmonic voltage than Load-A.

4. Figure 5.5 indicates that Load-A contributes harmonically consistently throughout the duration period. In the initial 20 seconds, Load-C has the greatest impact onto the 7th harmonic, but it reduces to a sixth of its preliminary participation in the final 30 seconds. In the latter 30 seconds, Load-B's participation to the 7th harmonic has grown. For the duration of the graph, Load-A's harmonic participation is about threefold more than that of Load-B.

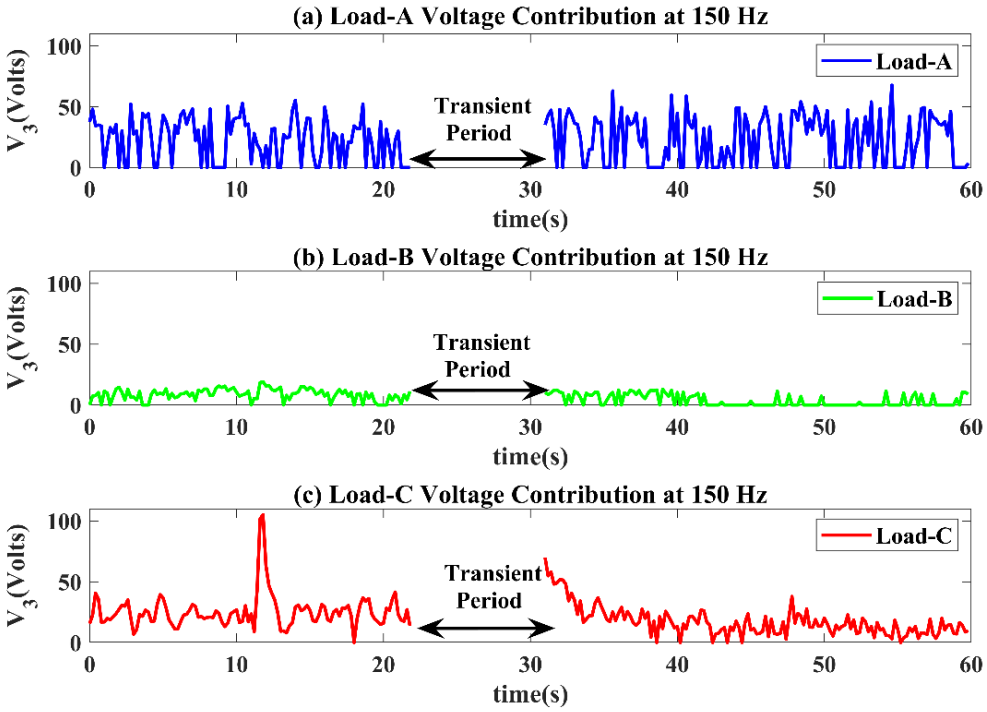

Figure 5.3. The contributions of Loads A, B, and C to the third order harmonic voltage observed at the PCC shown in Figure 3.6 are calculated and graphed in three ways: (a) depicts harmonic voltage participation of Load-A at 150 Hz (b) depicts harmonic voltage participation of Load-B at 150 Hz (c) depicts harmonic voltage participation of Load-C at 150 Hz, as calculated from field data.

5. Figure 5.6 depicts Load-A's current and voltage harmonic contributions. In Figure 5.6, the 5th and 7th voltage harmonic contributions of Load-A are twice as large as the contributions for the remaining harmonic orders. Current contributions to Load-A's 2nd and 5th harmonic orders are greater when compared to other harmonic orders, which is consistent with the approach presented in [11]. Even since [11] only shows current contributions and not voltage contributions, the voltage and current contributions from the same load are predicted to be closely related.

6. Figure 5.7 depicts Load-B's current and voltage harmonic contributions. Both the current and voltage harmonics have similar contribution patterns. Load-B has fewer non-stationary components than DC and AC arc furnaces, resulting in strongly correlated current and voltage contribution findings for all harmonics.

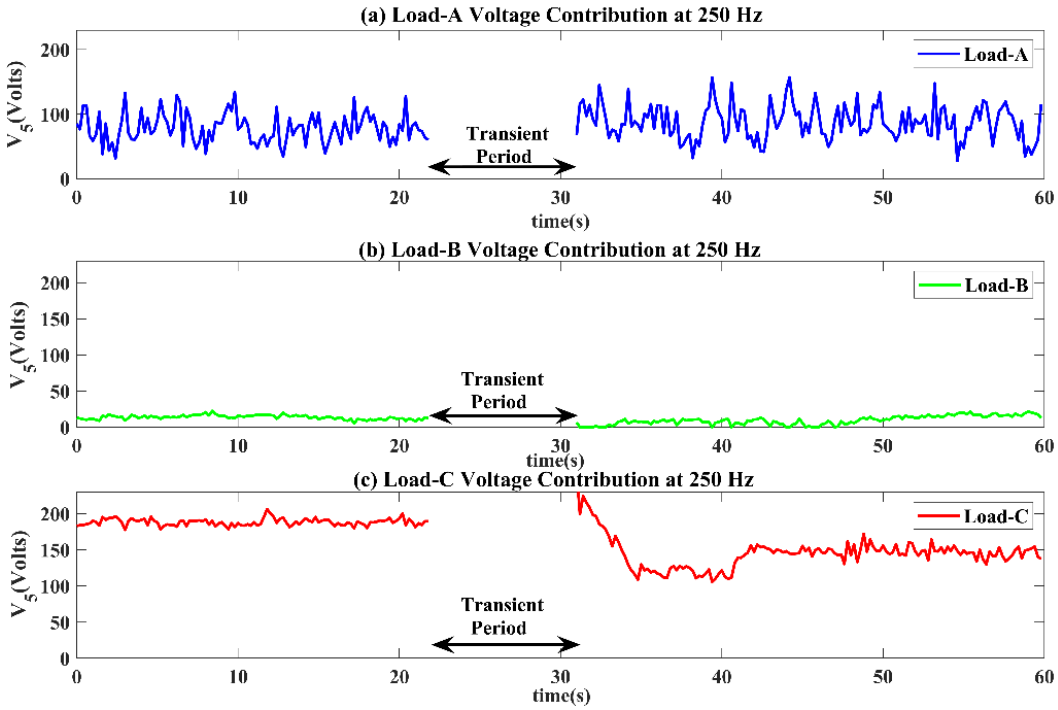

Figure 5.4. The contributions of Loads A, B, and C to the fifth order harmonic voltage observed at the PCC shown in Figure 3.6 is calculated and graphed in three ways: (a) depicts harmonic voltage participation of Load-A at 250 Hz (b) depicts harmonic voltage participation of Load-B at 250 Hz (c) depicts harmonic voltage participation of Load-C at 250 Hz, as calculated from field data.

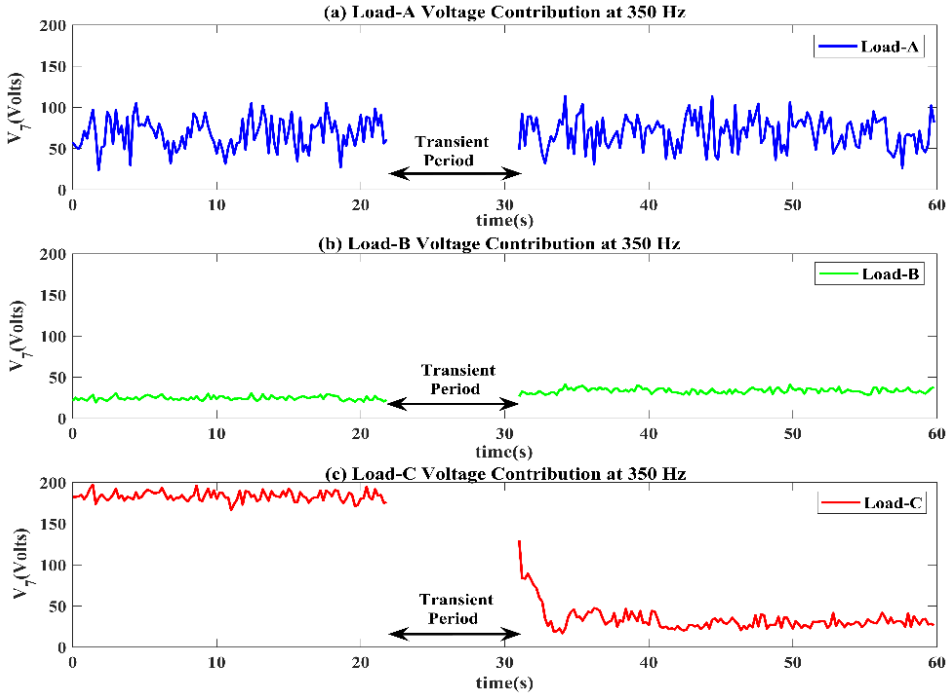

Figure 5.5. The contributions of Loads A, B, and C to the seventh order harmonic voltage observed at the PCC shown in Figure 3.6 is calculated and graphed in three ways: (a) depicts harmonic voltage participation of Load-A at 350 Hz (b) depicts harmonic voltage participation of Load-B at 350 Hz (c) depicts harmonic voltage participation of Load-C at 350 Hz, as calculated from field data.

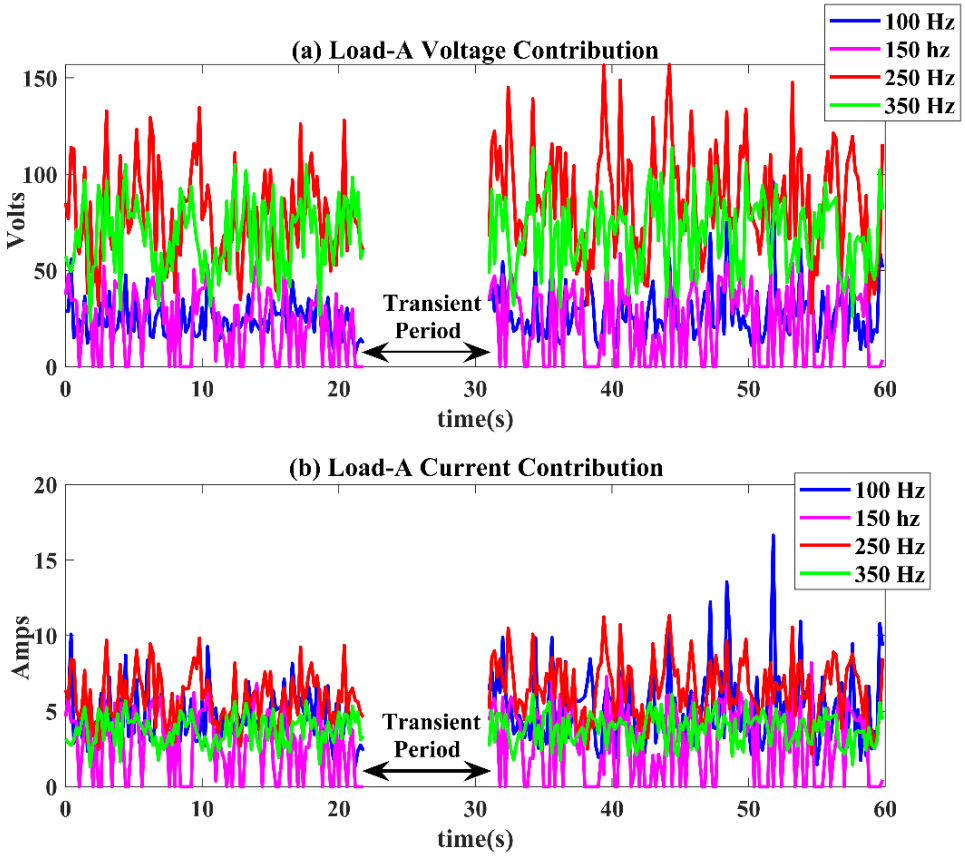

Figure 5.6. In Figure 3.6, the estimated harmonic contributions of current and voltage for Load-A within the PCC, (a) contribution of voltage for each harmonic order (b) contribution of current for each harmonic order.

7. Figure 5.8 depicts Load-C's harmonic participation to both voltage and current data. In the first twenty seconds of both voltage and current signals, Load-C contributes more to the 5^{th} and 7^{th} harmonic orders than other harmonics. However, Load-C contributes more to the 5^{th} harmonic voltage during the final 30 seconds compared to other harmonics. That is owing to the DC EAF's unsteady properties. The 2^{nd} current harmonic participation climbs to approximately ten amperes on average over the final 30 seconds, however the rise in the 5^{th} harmonic order is significantly smaller, reaching around two amperes at the start of the identical time. The findings indicate that Load-C plays a significant role in generating the 5^{th} harmonic current and voltage. Moreover, the analysis shows a strong correlation between the voltage and current contributions of Load-C throughout the entire measurement period.

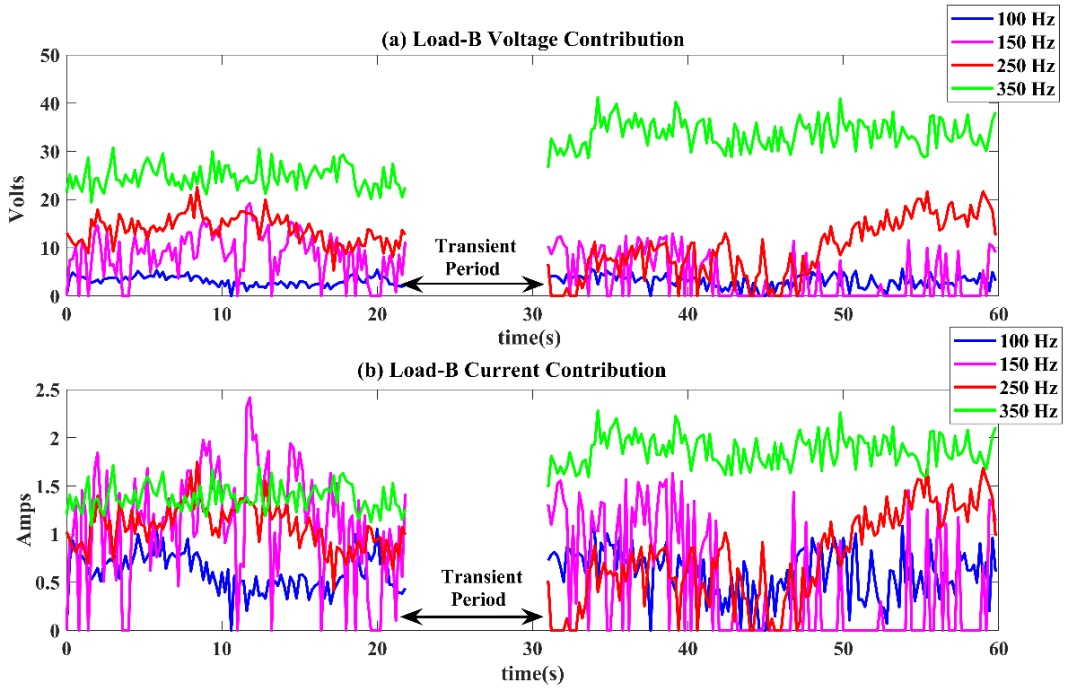

Figure 5.7. In Figure 3.6, the estimated harmonic contributions of current and voltage for Load-B within the PCC, (a) contribution of voltage for each harmonic order (b) contribution of current for each harmonic order.

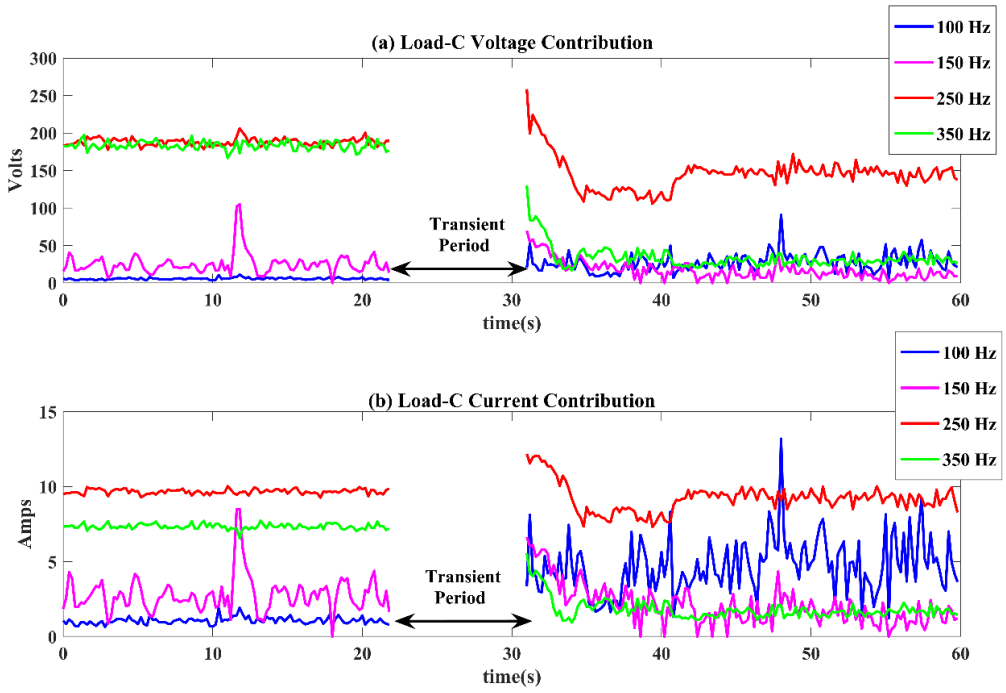

Figure 5.8. In Figure 3.6, the estimated harmonic contributions of current and voltage for Load-C within the PCC, (a) contribution of voltage for each harmonic order (b) contribution of current for each harmonic order.

6. THE IDENTIFICATION OF A VICTIM PLANT AT A PCC THROUGH WAVEFORM CORRELATION

The quantity of current harmonic contributions by arc furnace plants at the PCC voltage harmonic is calculated using the suggested technique for waveform correlation. For an affected facility with a well-designed compensation mechanism that filters out both its own harmonics and those from the upstream side, it might not, however, yield correct findings. This is because the victim plant's filter has minimal resistance to certain harmonics; therefore, assuming that other facilities linked to the PCC do not have filters or utilize filters with limited ability, harmonics generated by other facilities will pass through the filters of the victim facility. As a result of eliminating the harmonics that come from the upstream side, the electrical current recorded at the victim facility's feeder will be excessive. Since the victim facility takes in harmonics coming from the PCC, the excessive current observed at its feeder isn't a result of the plant's incapacity to allow its individual harmonics to pass through the PCC.

In such circumstances, the suggested analytical technique can be reinforced with a waveform relationship among the current recorded at the feeder and the current measured interior the facility. This approach can assist to identify whether the facility is a victim facility by studying the correlation among the feeder current data and the current data collected by the shunt harmonic filter, which can be acquired via on-site recordings.

In the simulation setting, many experimental conditions are built to explore the presence of predicted correlation links. The goal of such circumstances is to evaluate whether the facility is victimized by examining the relationship among filter and feeder currents. If a plant is victimized, there would be a strong association among these two currents. The relationship among filter and feeder currents would be minimal if every single plant had a unique filter and removed their individual harmonics.

As shown in Figures 6.1, 6.2 and 6.3, the simulation environment consists of four different simulations called Scenario-1, Scenario-2, Scenario-3 and Scenario-4. Evaluations for each scenario are made according to certain basic presumptions and the following procedures have been followed.

1. The investigation is carried out independently for each harmonic frequency. Table 6.1 displays the harmonic frequency amplitudes and phase angles for $I_{h,Supply}$, $I_{h,LoadA}$, and $I_{h,Load-B}$. The harmonics that result from the power facilities as well as the electrical supply are reflected in the line diagrams for the scenarios, which are thought to correspond to the quantities indicated in Table 6.1 at the start of the research. When a feeder has no current source, it signifies that the accompanying load does not contribute no harmonics into the network. Whether there is a presence of filters for various loads is investigated in order to examine several potential scenarios.

2. The nominal frequency of the system is fifty hertz; hence the 2^{nd} harmonic is equal to one hundred hertz. The data used for the simulation is constructed for a single minute interval at a sample rate of 25.6 kHz, that corresponds to the real-time measurements acquired in previous chapters.

3. I_{S1}, I_{L1}, I_{F1}, I_{S2}, I_{L2}, and I_{F2} are the currents that must be monitored in the field. In-plant measurements are for I_{L1}, I_{F1}, I_{L2}, and I_{F2}.

4. The IEC 61000-4-7 subgroup computing technique is used to construct the phase as well as magnitude spectra of measured currents with harmonics. This is repeated for each separate ten period DFT interval. Through inverse DFT, both phase and amplitude information are then used to generate the needed signals for the particular harmonic orders. It should be noted that in simulations with just one harmonic order, this approach could not be required. In real field experiments, however, every component of frequency is going to be superposed.

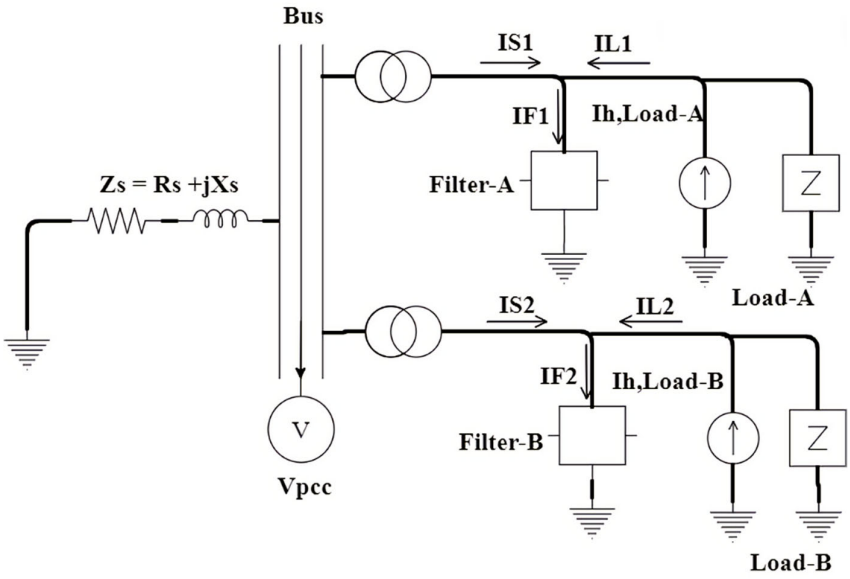

Figure 6.1. The electrical model's simplified schematic for verifying the proposed method is depicted as 1st Scenario.

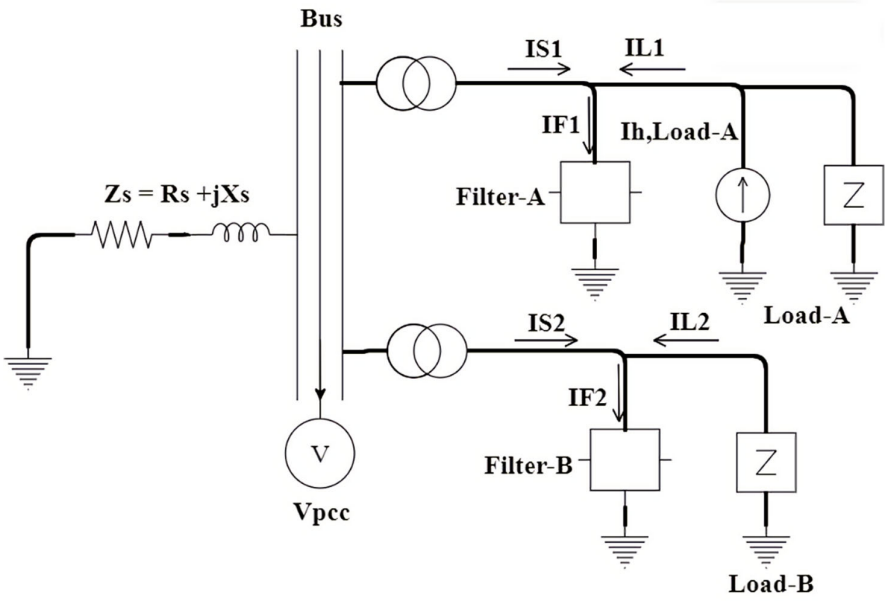

Figure 6.2. The electrical model's simplified schematic for verifying the proposed method is depicted as 2nd Scenario.

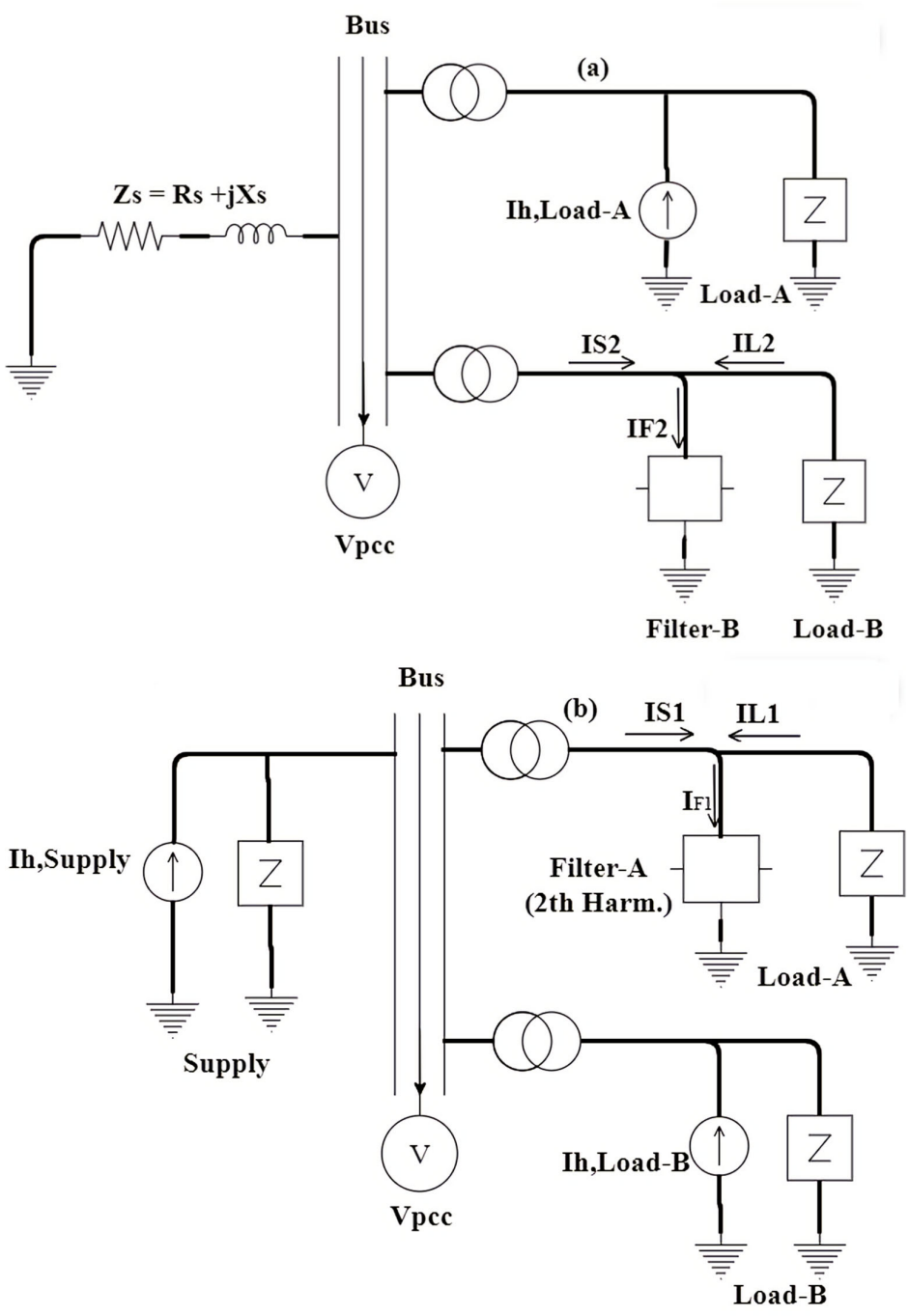

Figure 6.3. Scenarios 3 and 4 of the electrical model's simplified schematic for validating the suggested approach is shown. (a) 3rd Scenario and (b) 4th Scenario.

Table 6.1. The input values for magnitude and phase in the simulation scenario are expressed in per unit. Additionally, information regarding the filter condition is provided.

Sim. No	$I_{h,Supply}$	$I_{h,Load-A}$ (pu)	$I_{h,Load-B}$ (pu)	Filter-A	Filter-B
1	-	0.0074∟27.53°	0.0063∟49.5°	Exist	Exist
2	-	0.0039∟56.5°	-	Exist	Exist
3	-	0.0089∟-17.3°	-	Not Exist	Exist
4	0.0078∟40.5°	-	0.0039∟87.4°	Exist	Not Exist

5. Equation 4.6 is employed to compute the correlation coefficients among two current data for a given harmonic order.

6. Figures 6.4, 6.5, and 6.6 depict the outcomes of the correlation coefficients for each situation.

7. When a facility creates harmonics and has an acceptable harmonic filter, the correlation value among the current measured within the plant (I_L) and the current passing through the filter (I_F) is expected to be greater than the correlation value among filter current (I_F) and the upstream side current (I_S). If the majority of the current harmonics is generated on the upstream side, the reverse is predicted. As a result, by studying these relationships, it should be feasible to detect whether or not a facility is influenced by harmonics.

The outcomes of the simulations are presented as follows:

Scenario-1: In the first scenario, Load-A as well Load-B act as sources of 2nd harmonic current. Each load is equipped with a distinct 2nd harmonic filter. On the upstream side, no harmonic source is present. Table 6.1 contains the parameters used to generate the harmonic current data. Correlation coefficient values between recorded currents on both the load and source side are calculated and shown in Figure 6.4. The correlation coefficient between I_{L1}, I_{F1} and I_{L2}, I_{F2} is almost one as shown in Figure 6.4 (a) and (c). In contrast, the correlation coefficient between I_{S1}, I_{F1} and I_{S2}, I_{F2} is nearly zero as shown in Figure 6.4 (b) and (d). This outcome is in line with the expected outcome which indicates that the plants generate harmonics but are capable of filtering out their own harmonics.

Scenario-2: Scenario-2 is similar to Scenario-1, except that Load-B lacks an electric current supplier and all demands are equipped with harmonics filters. The findings are shown in

Figure 6.5. The correlation coefficient between I_{L1} and I_{F1} is almost one, indicating that Load-A plays a role for harmonic participation and that its filtering mechanism is working. I_{S1} and I_{F1} have a correlation coefficient that is close to zero. Load-B is a victim plant with a harmonic sinking problem because its harmonic filtration absorbs a substantial quantity of current with harmonics coming from Load-A. The correlation value among I_{L2} and I_{F2} is nearly zero, whereas the correlation value among I_{S2} and I_{F2} is close to 0.7, showing that Load-B is a victim plant.

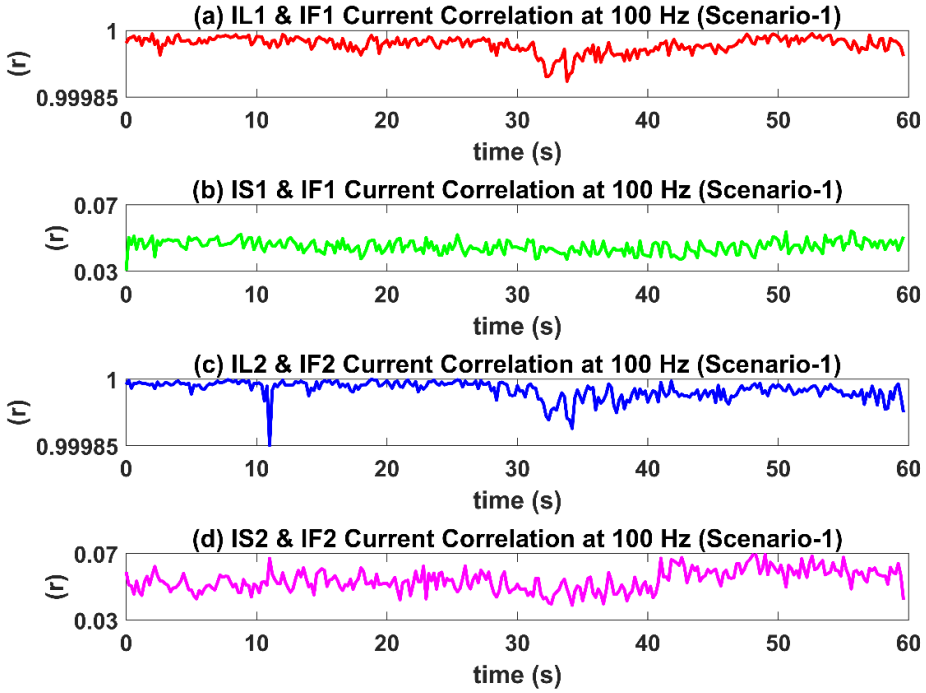

Figure 6.4. Scenario 1 correlation coefficient findings. (a) correlation coefficients between I_{L1} & I_{F1}, (b) correlation coefficients between I_{S1} & I_{F1}, (c) correlation coefficients between I_{L2} & I_{F2}, (d) correlation coefficients between I_{S2} & I_{F2}.

Scenario-3: As illustrated in Figure 6.3 (a), Load-A is an unfiltered harmonic current source, but Load-B has a filter but is not a harmonic current source and is a victim facility. Figures 6.6 (a) and (b) illustrate the correlation coefficients for the upstream (I_{S2}, I_{F2}) and downstream (I_{L2}, I_{F2}) sides. Based on the data provided, Load-A generates current harmonics at the PCC. However, Load-B's 2nd harmonic filter absorbs current harmonics originating from the upstream side, which leads to a failure in the facility.

Scenario-4: The harmonics in Figure 6.3 (b) are produced by the upstream side and Load-B, but only Load-A contains a 2nd harmonic filtration. Figures 6.6 (c) and (d) illustrate the

correlation values among I_{S1}, I_{F1}, and I_{L1}, I_{F1}. The correlation value among upstream side current and filter current is approximately one, while the correlation value among load current and filter current is practically zero. This implies the Load-A is victimized for the present situation. Based on these simulation results, it is concluded that correlation coefficients between feeders and inside facility recordings may be utilized to verify the suggested voltage participation calculation technique's outcomes if there's uncertainty regarding the facility having been a victimized, at the expense of inside facility measurements.

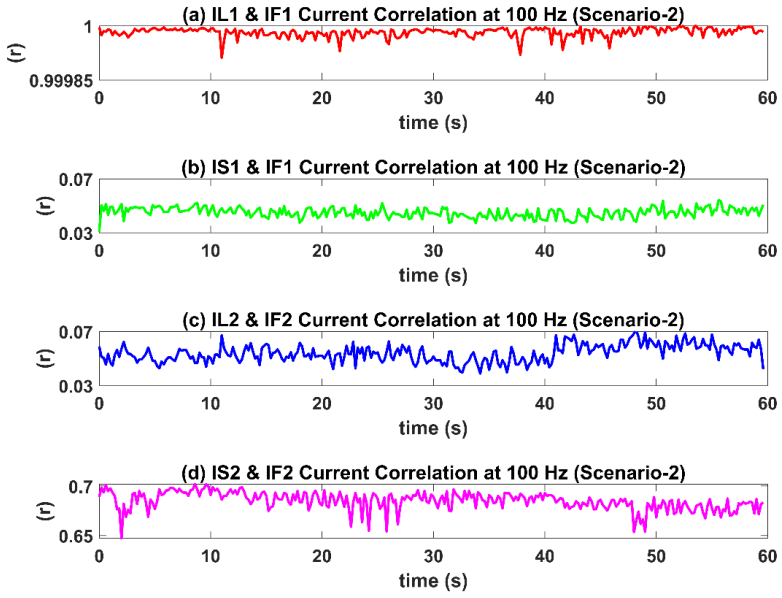

Figure 6.5. Scenario 2 correlation coefficient findings. (a) correlation coefficients between I_{L1} & I_{F1}, (b) correlation coefficients between I_{S1} & I_{F1}, (c) correlation coefficients between I_{L2} & I_{F2}, (d) correlation coefficients between I_{S2} & I_{F2}.

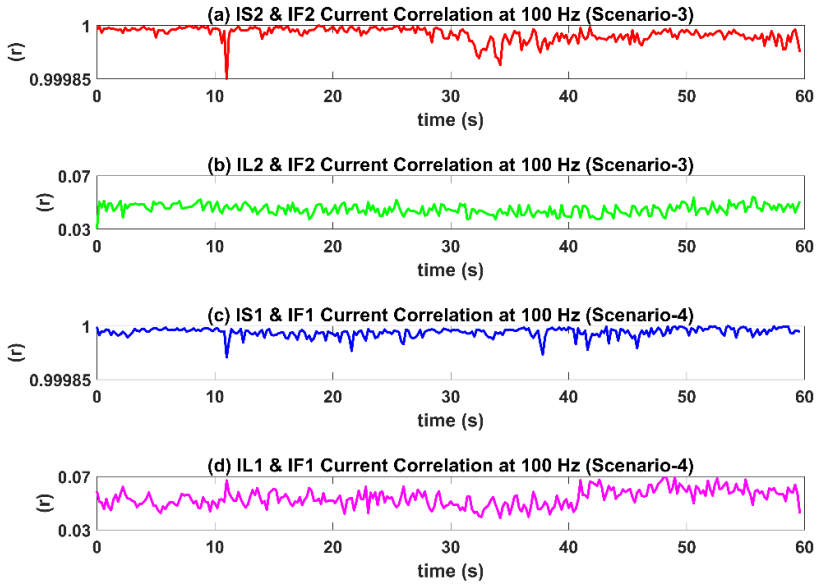

Figure 6.6. The correlation coefficient results for Scenario-3 and Scenario-4. (a) correlation

7. CONCLUSION

Two novel approaches for identifying harmonic current as well as voltage contributions in electrical power systems are proposed in this thesis. The first technique makes use of time domain signal correlation evaluation of concurrently collected voltage and current data from PQ+ monitors. It removes the requirement for immediate calculation of supply and demand impedance values, and it doesn't necessitate a network architecture for solving for harmonic participations, which reduces computing cost. The suggested technique is evaluated using PSCAD and MATLAB simulation instances, as well as real-measurement data acquired from steel manufacturing facilities interconnected to the network of transmissions. The findings indicate that the suggested approach is capable of identifying the current harmonic contribution of every facility in addition to the upstream side and that it may be employed in PQ tracking devices, active electrical power filtration systems and various other compensation mechanisms to avoid the disruptive impact of current harmonics and interharmonics.

The second approach presented in this thesis uses the waveform correlation of the observed feeder currents and the PCC voltage of the arc furnace facilities to calculate the specific quantities of voltage harmonics generated by the distinct feeders. This approach removes the requirement for immediate calculation of supplier and demand impedances, using only one observation or assessment of the provider line impedance given by the utility. The suggested technique has been verified utilizing scenarios generated in PSCAD and MATLAB, then confirmed by contrasting the real-world data results with those provided by other harmonic contribution technique employing identical field data set. According to the proposed technique, the voltage data measured in the PCC and only the corresponding EAF feeder current are required for real-time estimation of the contribution of the EAF to the PCC voltage, independent of the harmonic and interharmonic frequency. The suggested technique has been improved to identify a victim plant's harmonic current absorption problem using a strong compensating mechanism. Overall, the suggested approaches offer a chance to minimize the computing difficulty of harmonic accountability detection techniques while preventing the corruptive impact of present harmonics and interharmonics.

The present study employed real-time power quality data obtained from PQ+ devices that were developed within the National PQ Monitoring Project. The aim of this study is to identify the specific load(s) or utility(s) responsible for generating harmonic current and voltage in transformer substations (TS) using the proposed methods. By incorporating the algorithms developed in this thesis as additional software in PQ+ devices or other power quality measurement devices like PQ+s, the responsible parties for each TS can be identified quickly, thereby expediting the development process of relevant measures by the system operator. Ultimately, this will reduce the level of disruption caused on the grid. This thesis primarily aims to achieve this objective.

In the future, the goal is to extend the current study by incorporating a larger dataset and analyzing more transformer centers across the country for an extended period of time. Additional power quality event data will be obtained from the system operator, TEİAŞ, and the harmonic responsibility assessment algorithms are going to be upgraded appropriately. It will facilitate the identification of responsible loads per substation for harmonics, enabling prompt and effective development of relevant countermeasures by the system operator to minimize the impact of power quality events on the grid. Expanding the scope of this study is expected to be beneficial in terms of improving smart grid applications and developing strategies to counteract power quality events.

REFERENCES

1. International Electrotechnical Commission (2014). IEEE Recommended Practice and Requirements for Harmonic Control in Electric Power Systems. *IEEE Std 519-2014 (Revision of IEEE Std 519-1992)*, 1(1), 1-29.

2. Granaghan, M., and Beaulieu, B. (2006). Update on IEC 61000-3-6: Harmonic Emission Limits for Customers Connected to MV, HV, and EHV. *IEEE/PES Transmission and Distribution Conference and Exhibition, Dallas, TX, USA*, 1158-1161.

3. Xu, W., Liu, X. and Liu, Y. (2002). An Investigation on the Validity of Power Direction Method for Harmonic Source Determination. *IEEE Power Engineering Review*, 22(7), 62-62.

4. Cataliotti, A. and Cosentino, V. (2010). A New Measurement Method for the Detection of Harmonic Sources in Power Systems Based on the Approach of the IEEE Std. 1459–2000. *IEEE Transactions on Power Delivery*, 25(1), 332-340.

5. International Electrotechnical Commission, IEEE Standard Definitions for the Measurement of Electric Power Quantities Under Sinusoidal, Nonsinusoidal, Balanced, or Unbalanced Conditions (2010). *IEEE Std 1459-2010 (Revision of IEEE Std 1459-2000),*1(1),1-50.

6. Li, J., Fang, H., Liao, C. and Du, J. (2020). A New Method for Determination of Harmonic Responsibility Based on Quality Engineering Theory. *IEEE Access*, 8(1), 119071-119081.

7. Crovato, C. D. P., Goytia Mejia, R. I., and Righi, R. d. R. (2020). Toward Identifying Consumer Responsibility on Voltage Distortion and Filtering Based on the Maclaurin Series. *IEEE Transactions on Circuits and Systems II: Express Briefs*, 67(12), 3467-3471.

8. Safargholi, F., and Malekian, K. (2021). Relevant Factors for Evaluation of the Harmonic Responsibility of Utility and Customer. *IEEE Transactions on Power Delivery*, 36(1), 124-134, February 2021, doi: 10.1109/TPWRD.2020.2983256.

9. Yu, H. (2020). A Quantification Method of Harmonic Responsibilities Based on Current Tracing Principle. *7th International Conference on Information Science and Control Engineering (ICISCE)*, Changsha, China, 1614-1619.

10. Liu, H., Ma, T., Zhang, Y., Liu, S., and Wang, Y. (2022). Harmonic contribution determination based on change–point monitoring and shape context algorithm. *IET Geneation, Transmission Distribution*, 16(1), 453–466.

11. Unsar, O., Salor, O., Cadirci, I., and Ermis, M. (2014). Identification of harmonic current contributions of iron and steel plants based on time-synchronized field measurements–Part I: At PCC. *IEEE Transactions of Industry Applications*, 50(6), 4336–4347.

12. Unsar O., Salor, O., Cadirci, I., and Ermis, M. (2014). Identification of harmonic current contributions of iron and steel plants based on time-synchronized field measurements–Part II: Inside plants. *IEEE Transactions of Industrial Applications*, 50(6), 4348–4355.

13. International Electrotechnical Commission (2002), General Guide on Harmonics and Interharmonics Measurements for Power Supply Systems and Equipment Connected Thereto, IEC61000-4-7. *International Electrotechnical Commission Standard*, Geneva, Switzerland.

14. Pfajfar, T., Blazic, B., and Papic, I. (2007). Harmonic current vector method with reference impedances-field measurement verification. *9th International Conference on Electrical Power Quality and Utilization*, 1–6.

15. Xu, W., and Liu, Y. (2000). A method for determining customer and utility harmonic contributions at the point of common coupling. *IEEE Transactions on Power Delivery*, 15(2), 804–811.

16. Farhoodnea, M., Mohamed, A., Shareef, H., and Khan, R. (2010). An improved method for determining contribution of utility and customer harmonic distortions in a power distribution system. *International Journal on Electrical Engineering and Informatics*, 2(1), 204–215.

17. Zhou, F., Liu, F., Yang, R., Xiong, J., Liu, H., and Ding Z. (2019). A method for estimating multiple harmonic source parameters and responsibility division based on monitoring data without phase angle. *Proceedings IEEE Sustainable Power Energy Conference*, 2873–2878.

18. Yu, X., Liu, H., Wu, L., Gan, G., and Chen, S. (2021). A method of dividing harmonic responsibility based on total harmonic impedance. *4th International Conference on Energy, Electrical and Power Engineering (CEEPE)*, 998–1003.

19. Tang, K., and Shen, C. (2019). Method for detecting harmonic responsibility misjudgements based on waveform correlation analysis. *IET Generation, Transmission & Distribution*, 13(1), 1545–1554.

20. Internet: Electric arc furnace (2020). URL: https://en.wikipedia.org/wiki/EAF, Last Accessed: 07 February 2023.

21. Internet: Electric arc furnace (2020). URL: https://www.grecianmagne.com/EAF, Last Accessed: 07 February 2023.

22. Altıntaş, E. (2010). *Flicker Source Identification at a Point of Common Coupling of the Power System*, M.Sc. Thesis, The Graduate School of Natural and Applied Sciences of Middle East Technical University, Ankara.

23. Salor, Ö., and Çalışkan, M. (2020). Determination of Harmonic Current Responsibility at Point of Common Coupling of the Electrical System by Correlation of Voltage and Current Signals. *28th Signal Processing and Communications Applications Conference (SIU)*, Gaziantep, Turkey, 1-4.

24. Çalışkan, M., Salor, Ö., and Çiydem, M. (2021). Harmonic Contribution Detection of Iron and Steel Plants Based on Correlation of Time-Synchronized Current and Voltage Signals. *IEEE Industry Applications Society Annual Meeting (IAS),* Vancouver, BC, Canada, 1-8.

25. Çalışkan, M., Salor, Ö., and Çiydem, M. (2022). Waveform Correlation Based Harmonic Voltage Contribution Determination of Iron and Steel Plants Supplied From PCC. *IEEE Industry Applications Society Annual Meeting (IAS),* Detroit, MI, USA, 1-8.

26. Çalışkan, M., Salor, Ö., and Çiydem, M. (2022). Harmonic Contribution Detection of Iron and Steel Plants Based on Correlation of Time-Synchronized Current and Voltage Signals. *IEEE Transactions on Industry Applications,* 58(6), 8033-8044.

27. Çalışkan, M., Salor, Ö., and Çiydem, M. (2023). Waveform Correlation Based Harmonic Voltage Contribution Determination of Iron and Steel Plants Supplied From PCC. *IEEE Transactions on Industry Applications,* 59(4), 5178-5189.

28. Atalik, T. (2014). Multipurpose platform for power system monitoring and analysis with sample grid applications. *IEEE Transactions on Instrumentation and Measurement*, 63(3), 566–582.

29. Salor, Ö. (2009). Spectral correction-based method for interharmonics analysis of power signals with fundamental frequency deviation. *Electric Power System Research,* 79(7), 1025–1031.

30. Duric, M. B., and Durisic, Z. R. (2005). Frequency measurement in power networks in the presence of harmonics using Fourier and zero crossing technique. *Proceedings of IEEE Conference Russia Power Technology*, 1–6.

31. Jones, W. S., and Ness, A. (2003). Statistics at Square One. *International Journal of Epidemiology*, 32(1), 166–167.

32. Mutluer, H. B. (2008). *Design, Implementation and Engineering Aspects of TCR for Industrial SVC Systems*, Ph.D. Thesis, The Graduate School of Natural and Applied Sciences of Middle East Technical University, Ankara.

33. Demirci, T. (2011). Nationwide real-time monitoring system for electrical quantities and power quality of the electricity transmission system. *Generation, Transmission Distribution, IET*, 5(1), 540–550.

34. Altıntaş, E. (2010). A new flicker contribution tracing method based on individual reactive current components of multiple eafs at pcc. *IEEE Transactions on Industry Applications*, 46(5), 1746–1754.

35. Sonnemann, W. K., Wagner, C. L., and Rockefeller, G. D. (1958). Magnetizing Inrush Phenomena in Transformer Banks, *Transactions of the American Institute of Electrical Engineers. Part III: Power Apparatus and Systems,* 77(3), 884-892.

Gazili olmak ayrıcalıktır